Journal of Zhejiang University-SCIENCE B (Biomedicine & Biotechnology) *in press*
www.jzus.zju.edu.cn; www.springer.com/journal/11585
E-mail: jzus_b@zju.edu.cn

Research Article

https://doi.org/10.1631/jzus.B2600214

Drug repurposing: phenytoin sodium activates TBK1-dependent mitophagy to alleviate amyloid pathology and cognitive deficits in APP/PS1 mice

Ziyan CHEN[1,2*], Xufeng CEN[2*], Fengqi WANG[2,3], Jinyu ZHANG[1,2], Yanan TIAN[2], Manke ZHANG[2], Jie WU[4✉], Xiaoyan XU[2✉], Hongguang XIA[2✉1]

[1]*Department of Clinical Medicine, Zhejiang University School of Medicine, Hangzhou, 310003，China*

[2]*Research Center of Clinical Pharmacy of The First Affiliated Hospital & Liangzhu Laboratory, Zhejiang University School of Medicine, Hangzhou, 310003，China*

[3]*Department of Biochemistry, Zhejiang University School of Medicine, Hangzhou, 310003，China*

[4]*Zhejiang Key Laboratory of New Drug Development for Central Nervous System Diseases, Taizhou University, Taizhou, Zhejiang 318000, P. R. China*

Abstract: Alzheimer's disease (AD) is clinically characterized by progressive cognitive decline and pathologically by Aβ accumulation and tau aggregation. Current disease-modifying therapies remain limited, highlighting the need for brain-accessible agents that improve mitochondrial quality control. We screened more than 1000 FDA-approved drugs using an mt-Keima mitophagy reporter system and identified phenytoin sodium (PHT), a classical antiepileptic drug, as a candidate mitophagy inducer. In both cellular mitochondrial stress models and APP/PS1 mice, PHT ameliorated mitochondrial ultrastructural damage, partially stabilized mitochondrial membrane potential, improved mitochondrial respiratory activity and cell viability, reduced Aβ burden and neuronal apoptosis, and significantly improved cognition. Mechanistically, PHT enhanced TBK1 phosphorylation at Ser172 and promoted mitophagic flux; genetic knockdown of TBK1, pharmacological inhibition of TBK1 with amlexanox, or mitophagy inhibition with Mdivi-1 attenuated PHT's protective effects. Additional investigations in HeLa cells further suggested that PHT-associated mitochondrial clearance is not strictly dependent on Parkin and may involve TBK1-centered Parkin-independent mechanisms. These findings identify PHT as a clinically approved, brain-accessible compound that may alleviate AD-related pathology by enhancing TBK1-dependent mitochondrial quality control.

Key words: Alzheimer's disease; Phenytoin sodium; Mitophagy; TBK1; Drug repurposing

1 Introduction

Alzheimer's disease (AD), the most common neurodegenerative disorder, is clinically characterized by

* These authors contributed equally.
Ziyan Chen(https://orcid.org/0009-0008-3294-9567) and Xufeng Cen.

✉Corresponding Authors:
Jie Wu, jie_wu@fudan.edu.cn
Xiaoyan Xu, 0016751@zju.edu.cn
Hongguang Xia, hongguangxia@zju.edu.cn
Hongguang Xia, https://orcid.org/0000-0003-3044-9282

Received Apr. 4, 2026; Revision accepted May 30, 2026;
Crosschecked xxx. xx, 20xx; Published online xxx. xx, 20xx

progressively deteriorating memory impairment, language dysfunction, and executive decline (Palmqvist et al., 2021; Liu et al., 2022; Lau et al., 2023; Rizzo et al., 2023). Pathologically, AD is defined by the extracellular accumulation of β-amyloid (Aβ) into senile plaques, the intracellular aggregation of hyperphosphorylated tau into neurofibrillary tangles, and accompanying synaptic loss and neuronal death (Ising et al., 2019; Roda et al., 2022; Sehar et al., 2022). As insight into disease mechanisms has increased, AD is now widely recognized as a multifactorial, network-level syndrome in which neuroinflammation, oxidative stress, mitochondrial dysfunction, autophagy dysregulation, and vascular abnormalities converge across multiple pathological axes (Cen et al., 2020b; Leyane et al., 2022). Despite decades of research, disease-modifying therapies targeting Aβ or tau have achieved limited clinical success, highlighting the need to explore convergent pathogenic pathways driving AD progression and to identify novel therapeutic strategies(Cummings et al., 2016; Melchiorri et al., 2023; Zhang et al., 2023b; Zhang et al., 2025a).

The structural and functional integrity of mitochondria is essential for sustaining ATP production, calcium buffering, and cell survival. Mitophagy, a specialized form of selective autophagy, constitutes a central mechanism of mitochondrial quality control, targeting and eliminating damaged or superfluous mitochondria and thereby preserving mitochondrial homeostasis and cellular energetic balance(Lazarou M, 2015; Pickrell and Youle, 2015). A substantial body of evidence links impaired mitophagy to diverse neurodegenerative diseases, including AD, Parkinson's disease (PD), and Huntington's disease (HD), underscoring its pivotal role in maintaining neuronal health(Pickrell and Youle, 2015; Cen X, 2020; Cen et al., 2021b; Narendra Dp, 2024). Notably, mitophagy not only mediates basal mitochondrial turnover but is also indispensable for preserving synaptic function and delaying the progression of neurodegeneration(Pickrell and Youle, 2015; Cen, et al., 2020b; Cen, et al., 2021b). However, translating mitophagy-targeting strategies into clinical practice is hindered by the lack of safe, clinically available agents that can specifically activate mitophagy in the brain (Bourdenx et al., 2021; Cen, et al., 2021b; Mary et al., 2023).

Rather than a mere passive byproduct of AD progression, mitochondrial dysfunction is a critical driver within the pathogenic cascade(Young and Franklin, 2019; Yang et al., 2024). Mitochondrial damage promotes Aβ deposition, tau hyperphosphorylation, and neuronal apoptosis through multiple mechanisms, including impaired energy metabolism, excessive production of reactive oxygen species (ROS), and disruption of calcium homeostasis; these effects may be exerted even at preclinical stages of AD(Agrawal I, 2020; Misrani et al., 2021; Ashleigh et al., 2023; Wang et al., 2024a). Consequently, targeting mitophagy to improve mitochondrial homeostasis has emerged as a highly promising therapeutic strategy for AD. While numerous studies have demonstrated that mitophagy induction ameliorates both cognitive deficits and the pathological hallmarks of AD, no mitophagy-targeting drug has yet entered clinical trials for this disease(Bourdenx, et al., 2021; Cen et al., 2021a; Cen, et al., 2021b; Mary, et al., 2023). Motivated by this unmet need, drug repurposing, which leverages the extensive safety profiles of approved drugs, offers a cost-effective and time-efficient approach to identifying novel therapeutic agents for AD(Xu X, 2021; Zhang, et al., 2025a).

Mitophagy is regulated by multiple molecular pathways. In the canonical PINK1/Parkin pathway, mitochondrial depolarization stabilizes PINK1 on the outer mitochondrial membrane and recruits Parkin(Heo et al., 2015), leading to the ubiquitination of outer mitochondrial membrane proteins and the recruitment of autophagy receptors such as OPTN, NDP52, and p62/SQSTM1(Lazarou M, 2015; Pickrell and Youle, 2015; Kataura et al., 2023; Yao Z, 2023). Within this process, TBK1 is a central kinase; its activation enhances the ability of these receptors to recognize ubiquitinated mitochondria and interact with LC3/GABARAP proteins, thereby facilitating the autophagic engulfment of damaged mitochondria(Li et al., 2022; Yan et al., 2022; Zhang et al., 2023a; Tudorica et al., 2024).

In addition to the PINK1/Parkin pathway, several PINK1/Parkin-independent mechanisms contribute to mitochondrial quality control. Receptor-mediated pathways involving NIX, BNIP3, and FUNDC1 directly link mitochondria to LC3-family proteins through LC3-interacting region motifs, while mitochondrial dynamics influence the segregation and removal of damaged organelles (Um and Yun, 2017; Maeda et al., 2020; Marinković et al., 2021; Zhang, 2021). These parallel mechanisms highlight the complexity of mitophagy

regulation and establish a rationale for investigating TBK1 as a convergent regulator of mitochondrial clearance rather than focusing on a single linear pathway.

Phenytoin sodium (PHT), a classical antiepileptic drug first introduced into clinical practice in the 1930s and long used as a first-line therapy for partial seizures and generalized tonic-clonic seizures, was identified as a primary candidate. By blocking voltage-gated sodium channels, phenytoin stabilizes neuronal membranes and prevents the spread of abnormal discharges(D'arcy, 2024). Given its distinctive pharmacological profile, enduring clinical efficacy, and robust blood–brain barrier (BBB) penetration capacity—a critical prerequisite for AD therapeutics targeting central nervous system mitochondria—we selected PHT as the primary research and translational target for the present study(Andreux et al., 2019).

We first identified PHT as a potent activator of TBK1-dependent mitophagy through our approved drug screening. We then systematically evaluated the neuroprotective efficacy of PHT in both cell-based mitochondrial stress models and APP/PS1 transgenic mice and further delineated a TBK1-phosphorylation-centered mechanism linking PHT to enhanced mitophagy, reduced amyloid burden, and improved cognitive function. Our work identifies a clinically actionable candidate for rapid translation to AD therapy, provides compelling evidence for the therapeutic potential of mitophagy activators in AD, and deepens our understanding of the regulatory network of mitophagy in neurodegenerative diseases.

2 Methods and materials

2.1 Animal experiments

Four-month-old male C57BL/6J and APP/PS1 mice weighing 22–25 g were purchased from Jiangsu Ailingfei Biotechnology Co., Ltd. (Jiangsu, China). All animals were housed under specific pathogen-free conditions at the Experimental Animal Center of Zhejiang University. Two independent animal experiments were performed, and all mice received the corresponding treatments daily throughout the study period.

In Experiment 1, mice were randomly assigned to three groups: control (Ctrl), model (APP/PS1), and PHT (APP/PS1 mice treated with phenytoin sodium, 30 mg/kg every other day; catalog no. T0008, TargetMol). In Experiment 2, mice were randomly assigned to six groups: control (Ctrl), model (APP/PS1), PHT (APP/PS1 mice treated with phenytoin sodium, 30 mg/kg every other day), mitophagy inhibitor (APP/PS1 mice treated with Mdivi-1, 15 mg/kg every other day; catalog no. T1907, TargetMol), PHT + Mdivi-1 (APP/PS1 mice treated with Mdivi-1, 15 mg/kg every other day, plus phenytoin sodium, 30 mg/kg every other day), and PHT + TBK1 inhibitor (APP/PS1 mice treated with amlexanox, 15 mg/kg, every other day; catalog no. T1639, TargetMol, plus phenytoin sodium, 30 mg/kg, every other day).

Phenytoin sodium was administered at 10:00 a.m.; Mdivi-1 and amlexanox were administered at 2:00 p.m. All mice received 0.5% carboxymethyl cellulose (CMC) as the vehicle. All drugs were administered by gavage. The routes of administration and dosages were selected based on our previous work and the published literature. The treatment period lasted 90 days. All animal experiments were approved by the Laboratory Animal Welfare and Ethics Committee of Zhejiang University and conducted in strict accordance with institutional guidelines.

2.2 High-throughput screening for mitophagy inducers

To identify compounds that selectively enhance mitophagy under mitochondrial stress while preserving cellular and organellar integrity, we established a high-throughput screening platform using HEK293T cells stably expressing the pH-sensitive mitochondrial reporter mito-Keima (HEK293T-mito-Keima). Mitophagy flux was quantified as the percentage of cells exhibiting red fluorescence upon excitation at 560 nm, indicating mitochondrial delivery to acidic lysosomes, relative to the total cell count.

The screening workflow comprised four sequential tiers. First, more than 1000 FDA-approved compounds (TargetMol) were screened in triplicate under carbonyl cyanide m-chlorophenyl hydrazone

(CCCP)-induced mitochondrial damage to identify hits that significantly increased the proportion of red fluorescent cells. Second, primary hits were retested under basal conditions without CCCP to exclude compounds that induced mitophagy independently of mitochondrial stress and to ensure context-dependent specificity. Third, cytotoxicity was evaluated using the CellTiter-Glo Luminescent Cell Viability Assay (Promega), and compounds that caused a reduction in ATP-derived luminescence greater than 20% were excluded. Fourth, mitochondrial membrane potential ($\Delta\Psi m$) was assessed using TMRE staining, and compounds that induced more than 15% depolarization were eliminated to preserve basal bioenergetic function.

This integrated workflow incorporated functional efficacy, stress-responsive specificity, cytotoxicity thresholds, and mitochondrial physiological compatibility, thereby yielding rigorously validated candidate compounds suitable for subsequent mechanistic studies and in vivo therapeutic evaluation.

2.3 Behavioral testing

All behavioral tests were performed in a sound-attenuated enclosed room maintained at 22–25 °C with 45%–55% relative humidity under indirect illumination at 30 lux. Testing was conducted between 10:00 a.m. and 8:00 p.m. Animals were transferred to the testing room for habituation 24 h before behavioral testing commenced. Locomotor trajectories were recorded using an overhead camera and analyzed with ANY-maze 7.3 software. Following each test, the apparatus was wiped with 75% ethanol and allowed to dry before the next animal was assessed.

2.4 Morris water maze

A circular pool (120 cm in diameter and 50 cm in height) was filled to a depth of 30 cm with water maintained at 23 ± 1 °C; skim milk powder was added to render the water opaque. The escape platform was a 10-cm-diameter Plexiglas cylinder positioned in the center of the southwest quadrant and submerged 1 cm below the water surface.

Acquisition training was conducted over 5 consecutive days with four trials per day at 2-hour intervals. Starting positions were pseudo-randomized among quadrants I–IV. Mice that located the platform within 60 s remained on it for 15 s; those that did not were gently guided to the platform and were also allowed to remain there for 15 s. On day 6, a 60-s probe trial was conducted after platform removal. Latency to first enter the platform zone, time spent in the target quadrant, and number of platform crossings were recorded as indices of spatial reference memory.

2.5 Barnes maze

For the Barnes maze, we used a white PVC platform (92 cm in diameter) positioned 90 cm above the floor, which contained 20 equally spaced holes (5 cm in diameter). One hole was connected to a black escape box (20 cm × 8 cm × 8 cm), and its position remained fixed throughout the experiment. On day 0, mice were habituated by remaining in the escape box for 60 s, followed by free exploration of the maze for 4 min.

Acquisition training was performed on days 1–5, with two trials per day at 1-hour intervals. Before each trial, an opaque cube (15 cm × 15 cm × 15 cm) was placed in the center of the maze for 10 s. After removal of the cube, mice were allowed to explore for up to 180 s. Mice that entered the target hole remained in the escape box for 30 s. Mice that failed to locate the target hole were guided to the escape box and were also kept there for 30 s. Escape latency, primary errors (head pokes into non-target holes), and total travel distance were recorded.

On day 6, a 90-s probe trial was conducted after removing the escape box. Time spent in the target sector (a 45° cone-shaped area) and the distribution of search strategies (random, serial, or spatial) were analyzed.

2.6 Y-maze spontaneous alternation

A symmetrical gray PVC Y-maze with three identical arms (40 cm long, 9 cm wide, and 16 cm high) arranged 120° apart was used. Each mouse was placed at the distal end of one arm and allowed to explore freely

for 8 min. An arm entry was recorded when all four paws entered an arm. A spontaneous alternation was defined as three consecutive entries into three different arms. The spontaneous alternation rate (%) was calculated as follows: actual alternations/(total arm entries − 2) × 100. This parameter was used to evaluate spatial working memory.

2.7 Novel object recognition

The test arena comprised a white PVC open field measuring 40 cm × 40 cm × 40 cm. On day 1, mice were habituated to the empty arena for 5 min. On day 2, two identical objects (A1 and A2) were placed 10 cm from two diagonal corners, and exploration was recorded for 5 min. On day 3, one familiar object was replaced with a novel object of similar size but different shape and texture, and exploration was again recorded for 5 min.

Following each trial, the objects and the arena were cleaned with 75% ethanol. Exploration was defined as the mouse directing its nose toward an object within 2 cm, accompanied by gazing, sniffing, or touching. Climbing or sitting on the object was not considered exploration. The discrimination index (DI) was calculated as follows: (time spent exploring the novel object − time spent exploring the familiar object)/(time spent exploring the novel object + time spent exploring the familiar object).

2.8 Brain tissue pathology and ultrastructural examination

After 90 days of continuous treatment, mice were euthanized. Under deep anesthesia induced by 4% chloral hydrate (10 mL/kg, intraperitoneal injection), mice were perfused through the left ventricle into the ascending aorta with 0.01 M phosphate-buffered saline (PBS; pH 7.4, 37 °C) to remove blood. Whole brains were collected, photographed, and processed for subsequent analyses.

2.9 Paraffin embedding and hematoxylin-eosin staining

Samples were fixed in 4% paraformaldehyde (PFA) prepared in 0.1 M phosphate buffer (PB; pH 7.4) at 4 °C for no longer than 24 h. Tissues were dehydrated using a graded ethanol series (70%, 80%, 95%, and 100%; 1 h each), cleared in xylene (2 × 20 min), infiltrated with paraffin at 60 °C (melting point, 56–58 °C) for 2 h, and routinely embedded. Serial 4-μm sections were mounted at 45 °C and baked at 60 °C for 2 h.

Sections were deparaffinized in xylene (2 × 10 min), rehydrated using graded ethanol (100%, 95%, 80%, and 70%; 2 min each), rinsed in distilled water, and stained with hematoxylin and eosin. Hematoxylin staining was performed for 5 min, followed by bluing under running water for 5 min. Eosin staining was then performed for 1 min. Sections were subsequently dehydrated, cleared, mounted with neutral resin, and imaged using an Olympus BX53 microscope. Semi-quantitative image analysis was performed in a blinded manner using ImageJ.

2.10 Transmission electron microscopy

Samples were fixed in glutaraldehyde at 4 °C for 24 h, washed with 0.1 M PBS (3 × 15 min), post-fixed with 1% osmium tetroxide at 4 °C for 1 h, and washed again. Tissues were dehydrated through graded acetone (30%, 50%, 70%, 90%, and 100%; 15 min each), transitioned with propylene oxide (2 × 10 min), and infiltrated and embedded in Epon-812 resin at 37 °C for 12 h, at 45 °C for 12 h, and at 60 °C for 48 h.

Ultrathin sections (70 nm) were collected on copper grids and stained sequentially with 2% uranyl acetate for 10 min at room temperature and with 2.6% lead citrate for 5 min at room temperature. Images were acquired using a 120-kV transmission electron microscope. All samples were evaluated at ×11,000 magnification to assess the degree of mitochondrial damage. The injury score for each field was calculated as the ratio of damaged mitochondria to total mitochondria. Five randomly selected fields were analyzed for each sample, and the mean value was used as the mitochondrial injury score. Mitochondrial number was determined by direct counting in five randomly selected fields; the average value was used as the data point for each mouse.

2.11 Immunohistochemistry and immunofluorescence

Paraffin sections (5 μm) were deparaffinized in xylene and rehydrated through graded alcohols. Non-specific binding was blocked with rabbit serum for 30 min. Sections were then incubated overnight at 4 °C in a humidified chamber with the indicated primary antibodies. Following incubation with species-matched horseradish peroxidase-conjugated or fluorescent secondary antibodies, signals were developed or visualized in accordance with the corresponding protocols. Images were acquired for quantitative analysis of positive staining.

2.12 Mitochondrial membrane potential assay

Mitochondrial membrane potential was measured using a Rhodamine 123-based mitochondrial membrane potential assay kit (Beyotime, C2006). Cells were evenly seeded in live-cell imaging dishes and treated with the indicated drugs for 24 h. After one wash with PBS, 1 mL culture medium and 1 mL Rhodamine 123 working solution were added and mixed thoroughly, together with Hoechst dye (Beyotime, C1017). Following incubation at 37 °C for 20 min, the supernatant was discarded, cells were washed twice with PBS, fresh medium was added, and images were acquired using a HI-SIM fluorescence microscope.

2.13 Cellular ATP assay

Log-phase cells were seeded into black 96-well plates and cultured for 12 h to allow attachment. The medium was then replaced with 100 μL of fresh medium containing the corresponding drug or vehicle, and cells were incubated for 24 h. Cells were washed twice with pre-warmed PBS (37 °C), ATP assay reagent (Beyotime, S0027) was added, and the plates were incubated at room temperature for 20 min in the dark. After gentle washing to remove free background fluorescence, ATP signals were quantified using a Cytation 5 multimode plate reader.

2.14 Cell viability assay

Cell viability was determined using a CCK-8 assay kit (Lablead, CK001). Cells were seeded at a density of 8000 cells per well in 96-well plates and were then treated with CCCP, PHT, Mdivi-1, and/or amlexanox for 24 h. Subsequently, the CCK-8 working solution was added, and, after incubation at 37 °C for 1 h, absorbance was measured using a microplate reader (BioTek MQX200, Winooski, VT, USA). Cell viability (%) was calculated as follows: sample optical density (OD)/mean control OD × 100%.

2.15 Gene silencing

Log-phase cells were plated in 10-cm dishes and cultured at 37 °C in 5% CO2 until they reached approximately 70% confluence. si-TBK1 was mixed with RNAMIX and incubated with the cells for 6 h; the medium was then replaced, and the cells were cultured for an additional 72 h. Following confirmation of a marked reduction in TBK1 protein expression relative to the control group, subsequent experiments were conducted. The siRNA sequence targeting human TBK1 was as follows: sense, CCATGTGGGAGTTTATACAtt; antisense, TGTATAAACTCCCACATGGtt.

2.16 Immunofluorescence staining

Cells grown on coverslips were treated for 24 h, fixed with 4% PFA, blocked, and incubated with primary antibodies against TOM20 and phospho-TBK1 (p-TBK1), followed by the corresponding fluorescent secondary antibodies. Slides were mounted with DAPI-containing mounting medium and imaged using the HI-SIM system. Fluorescence intensity and signal area were quantified using ImageJ.

2.17 Mitochondria-lysosome co-localization in live cells

For live-cell imaging of mitochondria-lysosome co-localization, log-phase cells were seeded at a uniform density into 35-mm glass-bottom confocal dishes (20 mm diameter, No. 1.5H) and cultured for 12 h until the

adherent area reached at least 50%, followed by 24 h of drug treatment. MitoTracker Deep Red FM (Thermo, A66440), LysoTracker Green FM (Thermo, A66441), and Hoechst working solutions were prepared and protected from light.

After one wash with pre-warmed PBS, 1 mL of the staining mixture was added, and cells were incubated at 37 °C in 5% CO2 for 20 min. The staining solution was then removed, cells were washed twice with PBS, and 1 mL of medium was retained for imaging. Co-localization was quantified using ImageJ.

2.18 Western blot analysis

Tissues or cells were lysed in ice-cold RIPA buffer supplemented with protease and phosphatase inhibitors. After sonication, lysates were centrifuged at 12,000 × g for 10 min. Protein concentrations were determined using the bicinchoninic acid (BCA) assay. Equal amounts of protein were separated by sodium dodecyl sulfate–polyacrylamide gel electrophoresis (SDS-PAGE) and transferred onto PVDF membranes. Membranes were blocked with 5% non-fat milk for 1 h and then incubated overnight at 4 °C with primary antibodies against PRKN, PINK1, TOM20, TIM23, SQSTM1/p62, TBK1, phospho-TBK1, CALNEXIN, LC3, BNIP3, and TUBULIN (all at 1:1000 dilution). Protein bands were visualized using enhanced chemiluminescence (ECL) reagents, and band intensities were quantified using ImageJ. Relative protein expression was calculated as the grayscale value of the target protein normalized to ACTB/β-actin. For the supplemental HeLa cell experiments, lysates were prepared from control, mitochondrial stress, and mitochondrial stress + PHT groups and analyzed for p-TBK1, total TBK1, TIM23, NIX, FUNDC1, and β-tubulin.

2.19 Antibodies

The following antibodies were used for Western blotting and immunofluorescence analyses: β-tubulin (#M1305-2); TOM20 (#42406, Cell Signaling); TIM23 (#34822, Cell Signaling); P62 (#23214, Cell Signaling); TBK1/NAK (#3504S, Cell Signaling); phospho-TBK1/NAK (Ser172) (#5483S, Cell Signaling); CALNEXIN (#2433S, Cell Signaling); APP (#4000000465, ABclonal); NIX and FUNDC1 antibodies for supplemental Western blotting. Secondary antibodies used for Western blotting and immunofluorescence included goat anti-mouse (#31430, Thermo Fisher Scientific, Waltham, MA, USA), goat anti-rabbit (#31460, Thermo Fisher Scientific), goat anti-rabbit Alexa Fluor 568 (#A-11011, Thermo Fisher Scientific), goat anti-mouse Alexa Fluor 488 (#A-11029, Thermo Fisher Scientific), goat anti-rabbit Alexa Fluor 488 (#A-11008, Thermo Fisher Scientific), goat anti-rabbit Alexa Fluor 555 (#A-21248, Thermo Fisher Scientific), and goat anti-rabbit Alexa Fluor 647 (#A-21245, Thermo Fisher Scientific).

2.20 Mitochondrial quality score

To quantify ultrastructural mitochondrial damage, a four-level mitochondrial quality score (MQS) system was used, ranging from 0 (healthy) to 3 (severely damaged). One point was assigned for each of the following features, with a maximum total score of 3: vacuolation (at least one obvious electron-lucent vacuole in the matrix), membrane rupture (at least one discontinuity in the outer or inner membrane), and crista loss (greater than 50% loss or fragmentation of cristae).

Five non-overlapping fields were randomly selected from each electron micrograph. Two investigators independently scored individual mitochondria in a blinded manner. The MQS for each field was calculated as the average score across all mitochondria in that field and was used for subsequent statistical analysis.

2.21 Statistical analysis

Experimental data were analyzed using ImageJ, GraphPad Prism 8.0.2, SPSS 22.0, and Origin 2021. Data are presented as mean ± SD. One-way analysis of variance (ANOVA) followed by Duncan's multiple comparisons test was used where appropriate. Pearson correlation analysis was performed using Origin 2021.

3 Results

3.1 Phenytoin sodium alleviates cognitive and pathological phenotypes related to AD in APP/PS1 mice

Accumulating evidence indicates that mitophagy activation can alleviate the pathological phenotypes of AD, as illustrated in Figs. S1A and S1B. Specifically, we first conducted a primary screen to identify drugs capable of inducing mitophagy under mitochondrial-damage conditions. In the second round of screening, we evaluated the effects of these candidate drugs on normal mitochondria. Finally, to exclude off-target effects, we assessed mitochondrial membrane potential and cytotoxicity. We identified several mitophagy-inducing drugs through this rigorous screening pipeline (Figs. S1C and S1D). Given that therapeutic agents targeting AD must cross the BBB to exert central neuroprotective effects, we selected PHT, which exhibited robust mitophagy-inducing efficacy and strong BBB penetration capacity, as the primary research and translational target in the present study. To determine whether PHT exerts therapeutic effects on AD, we first evaluated its impact on cognitive deficits and pathological hallmarks using APP/PS1 transgenic mice, a well-validated murine model of Aβ-driven AD. Following a 3-month treatment with PHT, behavioral tests were conducted with APP/PS1 mice and pathological analyses of their brain tissue were performed (Fig. 1A).

Spatial learning and memory, the core cognitive functions impaired in AD, were evaluated using the Morris water maze (MWM) test. During the acquisition phase, vehicle-treated APP/PS1 mice exhibited significantly prolonged escape latency compared with wild-type (WT) littermates (Figs. 1B and 1C), indicating severe spatial learning impairment. On the probe/test trial, vehicle-treated APP/PS1 mice spent substantially less time in the target quadrant, confirming defective spatial memory. Conversely, PHT treatment significantly shortened the escape latency of APP/PS1 mice to a level comparable to that of WT mice and markedly increased the time spent exploring the target quadrant, demonstrating a robust ameliorative effect of PHT on AD-related cognitive deficits (Fig. 1D).

Consistent with the cognitive improvement, PHT treatment effectively attenuated AD-related pathological damage in the hippocampus and cortex, the brain regions most susceptible to neurodegeneration in AD. Enzyme-linked immunosorbent assay (ELISA) results showed that insoluble Aβ was reduced in the PHT group compared with the APP/PS1 group (Fig. 1E). Immunofluorescence further demonstrated that PHT significantly inhibited neuronal apoptosis—a key feature of AD pathogenesis—as evidenced by a reduction in TUNEL-positive neurons (Fig. 1F). PHT administration significantly reduced the number of Aβ plaques in APP/PS1 mice compared with vehicle controls (Fig. 1G). Collectively, these data indicate that PHT can induce mitophagy of damaged mitochondria and effectively alleviate AD-related cognitive and pathological phenotypes.

3.2 PHT improves mitochondrial structural integrity and specific functional readouts in AD models

PHT effectively ameliorates cognitive deficits and AD-related pathological phenotypes in APP/PS1 mice. Because mitochondrial dysfunction is a central pathogenic event in AD and is closely linked to the in vivo neuroprotective effects of PHT, we next investigated the organellar basis of this protection, specifically, whether PHT improves mitochondrial structural and functional integrity.

We performed transmission electron microscopy (TEM) analysis on mouse brain tissue to explore whether PHT-mediated phenotypic improvement is associated with mitochondrial structural protection. As illustrated in Fig. 2A, the mitochondria in the neurons of untreated APP/PS1 mice exhibited severe ultrastructural damage, including widespread vacuolization, cristae fragmentation, and even outer membrane rupture. PHT intervention improved mitochondrial morphology, with more tightly organized cristae and relatively intact membrane structures. The mitochondrial health score was significantly higher in the PHT-treated group than in the model control group (Fig. 2B, $P < 0.001$), and mitochondrial quality improved toward WT levels,

supporting the conclusion that PHT ameliorates mitochondrial structural damage in APP/PS1 mice in vivo.

Building on these in vivo structural findings, we validated PHT's protective effects on mitochondrial respiratory activity in vitro using an inducible APP overexpression model established in 293T cells—a key cellular model that mimics AD-related APP overload. Using the Seahorse XF real-time energy metabolism analysis system, we measured mitochondrial respiratory chain function. PHT partially reversed the inhibition of mitochondrial oxidative phosphorylation induced by APP overexpression and improved cellular energy homeostasis (Fig. 2C), providing functional evidence of PHT-mediated mitochondrial protection under AD-relevant conditions.

Given that Δψm is a core determinant of mitochondrial function and is closely associated with oxidative phosphorylation, we further explored whether PHT modulates Δψm using 293T cells. Employing the rhodamine 123 fluorescent probe and the Olympus FV3000 laser confocal microscope (Figs. 2D and 2E), we found that combining oligomycin A + antimycin A (O/A) led to a rapid loss of Δψm and sustained depolarization, a feature characteristic of mitochondrial dysfunction. In contrast, PHT administration resulted in a gradual recovery of Δψm; although full restoration to the control level was not achieved, the recovery trend was distinct and reproducible, indicating that PHT effectively stabilizes Δψm under mitochondrial stress conditions.

To confirm the association between improvement in mitochondrial structural and functional readouts and cytoprotection, we evaluated PHT in AD-relevant cellular toxicity models. In the SH-SY5Y neuronal cell line injured by the Aβ35-45 peptide fragment—a well-validated model of AD-related neurotoxicity—PHT treatment significantly improved cell viability (Fig. 2F). Similarly, in the CCCP-induced acute mitochondrial depolarization model, the CCK-8 assay results showed that PHT effectively attenuated the reduction in cell viability (Fig. 2G). These findings confirm the consistency of PHT's protective effects across multiple in vitro models of mitochondrial dysfunction and neurotoxicity.

Collectively, these results demonstrate that PHT improves mitochondrial structural integrity and specific functional readouts in AD models. In vivo, PHT ameliorates mitochondrial ultrastructural damage in APP/PS1 mice. In vitro, PHT improves APP-induced mitochondrial respiratory impairment, partially stabilizes Δψm, and enhances cell viability.

3.3 PHT induces mitophagic flux to clear damaged mitochondria in AD models

To systematically elucidate whether PHT mediates its neuroprotective effects through mitophagy activation, we first evaluated its impact on mitophagic flux in cellular models of mitochondrial stress.

Western blot analysis demonstrated that following 72-hour exposure to Aβ35-45 to establish an in vitro neuronal stress model, treatment of HEK293T cells with PHT (10 μmol/L) alone significantly reduced the expression of the mitochondrial outer membrane protein TOMM20, with no change in the loading control Tubulin (Fig. 3A). We then assessed whether PHT could enhance stress-induced mitophagy using the mitochondrial uncoupler CCCP. Treatment with CCCP (3 μM) alone significantly decreased TOMM20 levels, and co-treatment with PHT (10 μM) led to a further reduction in TOMM20 abundance (Fig. 3A). These results indicate that PHT promotes mitophagy in both Aβ35-45-induced and CCCP-induced cellular stress models.

To provide further functional evidence for PHT-induced mitophagy, we performed experiments in cells stably expressing the pH-sensitive mitochondria-targeted probe. Keima primarily emits green fluorescence (Ex = 438 nm) in a neutral environment (i.e., mitochondria) but shifts to red fluorescence (Ex = 586 nm) in the acidic lumen of lysosomes; the red/green fluorescence ratio therefore specifically reflects the degree of mitochondrial delivery to lysosomes. PHT co-treatment significantly increased the number of red puncta and the red/green fluorescence ratio (Fig. 3B), confirming that PHT promotes the delivery of damaged mitochondria to lysosomes and enhances functional mitophagic flux.

To verify this effect at the ultrastructural level, we performed TEM observations of cells in each treatment group. In the control group, mitochondria exhibited intact morphology with dense cristae; CCCP treatment induced typical damage, including rupture of the outer membrane and matrix vacuolization. PHT

co-treatment significantly alleviated these pathological changes and restored mitochondrial structural integrity. Notably, when autophagosome-lysosome degradation was blocked by pre-treatment with the lysosomal acidification inhibitor bafilomycin A1 (BafA1, 100 nM, 6 h), PHT's protective effect was significantly attenuated, and mitochondrial damage reappeared (Fig. 3C). More importantly, a large number of double-membrane mitophagosomes encapsulating mitochondria were observed in the group co-treated with PHT and BafA1 (Fig. 3D), and the mitochondrial health score was significantly lower than that in the group treated with PHT alone (Fig. 3E). These findings indicate that PHT actively promotes the recognition and autophagosome encapsulation of damaged mitochondria, and the blockage of lysosomal function leads to the accumulation of intermediate mitophagic structures; this "upstream activation and downstream blockage" phenotype confirms that PHT preserves mitochondrial homeostasis by enhancing selective mitophagy.

We performed confocal imaging with MitoTracker Deep Red and LysoTracker Green double-staining and quantified the Pearson colocalization coefficient to dynamically track mitochondria–lysosome interactions at the live-cell level. CCCP treatment caused only a mild increase in colocalization signals, whereas PHT co-treatment significantly enhanced the spatial overlap between mitochondria and lysosomes (Figs. 3F and 3G). This effect was completely blocked by pre-treatment with Mdivi-1 (10 μM, 12 h), a mitochondrial fission inhibitor, indicating that the selective mitophagy promoted by PHT depends on Drp1-mediated mitochondrial fragmentation.

Finally, the functional relevance of PHT-induced mitophagy was validated using cell viability. The CCK-8 assay results showed that PHT significantly ameliorated the CCCP-induced reduction in cell viability; however, pretreatment with Mdivi-1 completely reversed this protective effect (Fig. 3H), demonstrating that the integrity of the mitophagic pathway is a key determinant of PHT's cytoprotective effect.

Collectively, these data demonstrate that PHT promotes selective mitophagy through a Drp1-associated mechanism, facilitating the recognition, encapsulation, and lysosomal degradation of dysfunctional mitochondria, thereby improving mitochondrial structural and functional homeostasis and exerting neuroprotective effects.

3.4 TBK1 mediates PHT-induced mitophagy and mitochondrial homeostasis

We first detected key regulatory nodes to systematically dissect the upstream molecular mechanism by which PHT induces mitophagy. Western blot analysis demonstrated that in the context of mitochondrial damage induced by CCCP (3 μmol/L), PHT (10 μmol/L) treatment significantly enhanced TBK1 phosphorylation at Ser172 without altering the expression level of total TBK1 protein (Fig. 4A). This suggests that, rather than regulating TBK1 expression, PHT triggers a "stress-responsive" signal transduction by rapidly activating TBK1 kinase activity, thereby promoting mitophagy.

Based on this biochemical finding, we further visualized TBK1's subcellular activation dynamics. We performed super-resolution immunofluorescence imaging of p-TBK1 (Ser172) using high-inclination super-resolution structured illumination microscopy (Hi-SIM). The results showed that CCCP treatment alone induced only a small amount of diffuse p-TBK1 punctate signals. Conversely, combined treatment with CCCP and PHT significantly enhanced p-TBK1 fluorescence intensity in the perinuclear region and cytoplasm, consistent with a typical stress-activation pattern. Notably, this phosphorylated signal almost completely disappeared in TBK1-knockdown cells (Figs. 4B and 4C), which not only verified the antibody specificity but also confirmed the spatial dependence of PHT-induced TBK1 activation on sufficient protein substrates. Together, these biochemical and imaging data point to TBK1 as a key molecular target of PHT action.

To further explore whether TBK1 is involved in the directed recruitment of damaged mitochondria to lysosomes, we performed MitoTracker Deep Red and LysoTracker Green double-staining, combined with high-resolution confocal microscopy, to quantitatively assess the spatial colocalization coefficient between mitochondria and lysosomes. In control cells, PHT significantly increased colocalization between the two after CCCP damage, indicating that dysfunctional mitochondria were effectively delivered to lysosomes. In

contrast, after TBK1 knockdown, the degree of this colocalization was significantly reduced (Fig. 4D–E), indicating that PHT relies on TBK1 to complete the selective recognition and targeted clearance of damaged mitochondria.

To provide direct evidence of functional mitophagic flux, we introduced the specific TBK1 inhibitor Amlexanox (20 μM) into 293T cells stably expressing the pH-sensitive probe mito-Keima. Because Keima mainly emits green fluorescence in the neutral mitochondrial environment but shifts to red fluorescence in the acidic lysosomal lumen, its red/green ratio can specifically reflect mitophagic flux. Amlexanox completely inhibited the PHT-induced increase in the red/green fluorescence ratio (Fig. 4F), further confirming that TBK1 kinase activity is the rate-limiting step for PHT to activate functional mitophagy.

Given that one downstream effect of mitophagy is the maintenance of mitochondrial membrane integrity, we subsequently evaluated the role of TBK1 in the PHT-mediated restoration of Δψm. Following acute depolarization induced by combined treatment with oligomycin A and antimycin A (O/A), a partial but significant recovery of Δψm was observed in control cells after PHT intervention. In contrast, PHT completely lost this restorative effect in TBK1-knockdown cells (Figs. 4G and 4H), indicating that TBK1 not only regulates mitophagic flux but also directly participates in the PHT-mediated maintenance of mitochondrial electrochemical homeostasis.

Consistent with this, we further investigated the functional significance of TBK1 in energy metabolism. In 293T cells overexpressing human APP under the background of TBK1 knockdown, APP overexpression significantly inhibited the basal oxygen consumption rate (OCR), ATP production-related OCR, and maximum respiratory capacity. PHT significantly reversed the above inhibition in control cells, but its ability to improve mitochondrial oxidative phosphorylation was completely abolished in the absence of TBK1 (Fig. 4I).

Finally, we performed terminal phenotypic verification across multiple independent systems to comprehensively evaluate the functional necessity of TBK1 in the neuroprotective effect of PHT. The CCK-8 cell viability assay showed that PHT failed to reverse the decrease in cell viability caused by CCCP (3μM) in either TBK1-knockdown or WT cells pretreated with amlexanox (Figs. 4J and 4K). This result is highly consistent with the aforementioned autophagy, membrane potential, and metabolic data, forming a complete causal chain of evidence from molecular activation to cellular function(Zhou et al., 2025).

Collectively, these data demonstrate that PHT rapidly enhances TBK1 phosphorylation and drives the mitophagic pathway, thereby improving membrane potential, energy metabolism, and cell viability. TBK1 serves as a core molecular hub for PHT, enabling its regulation of mitochondrial homeostasis and exerting neuroprotective effects.

To further clarify whether PHT-induced mitophagy is strictly dependent on the canonical PINK1/Parkin pathway, we conducted additional experiments in HeLa cells, a cellular background commonly used in Parkin-independent mitophagy studies. Under mitochondrial stress conditions, PHT still enhanced TBK1 phosphorylation and further reduced TIM23 abundance compared with the model group (Fig. S2). NIX and FUNDC1 were increased after modeling, but PHT treatment did not further elevate their total protein levels. These findings suggest that PHT can promote TBK1-associated mitochondrial clearance in a Parkin-independent cellular context, but this effect cannot be simply explained by increased total NIX or FUNDC1 expression.

3.5 TBK1-dependent mitophagy mediates PHT-induced cognitive improvement and pathological amelioration in APP/PS1 mice

We conducted systematic intervention studies in APP/PS1 double-transgenic mice to determine whether PHT-promoted mitophagy depends on TBK1 phosphorylation in vivo. Mice were administered PHT (30 mg·kg−1) by oral gavage every other day for 3 consecutive months, and some animals were concurrently administered the TBK1 inhibitor amlexanox or the mitophagy inhibitor Mdivi-1 to evaluate the functional necessity of the TBK1 signaling pathway.

Behavioral assessments revealed that APP/PS1 mice exhibited persistently elevated target-finding laten-

cy during Barnes maze training, indicating significant impairment in spatial learning ability. In contrast, the PHT-treated group exhibited a marked reduction in latency as training days progressed (Fig. 5A). Although latency did not fully recover to WT levels, it was significantly superior to that of the model group. Notably, this ameliorative effect was completely abolished when amlexanox or Mdivi-1 was co-administered, and the learning curve reverted to the level of the model group (Fig. 5B). In the probe trial, the PHT group showed a reduction in the number of incorrect hole entries (Fig. 5C), a significant increase in the proportion of time spent in the target quadrant (Fig. 5D), and a marked shortening of the time to first enter the target hole (Fig. 5E); however, these advantages were lost in the inhibitor co-treatment groups. Similarly, PHT significantly increased the novelty preference index and working memory accuracy in the novel object recognition test (Fig. 5F) and the Y-maze spontaneous alternation task (Fig. 5G), whereas both inhibitors reversed cognitive performance to the impaired baseline. Collectively, these results demonstrate that the pro-cognitive effect of PHT is strictly dependent on TBK1 activity and functional mitophagy.

The behavioral improvements described above were highly consistent with reductions in neuropathological changes. TEM analysis demonstrated that PHT significantly restored mitochondrial cristae density and membrane integrity in the hippocampal neurons of APP/PS1 mice. However, co-administration of amlexanox or Mdivi-1 exacerbated mitochondrial vacuolization and cristae fragmentation, with ultrastructural indicators indistinguishable from those of the untreated model group (Figs. 6A and 6B), suggesting that an intact TBK1-mitophagy axis is required to support PHT's mitochondrial protective effect. Immunofluorescence staining further revealed that PHT significantly reduced the intensity of Aβ deposition in the hippocampus, whereas amlexanox co-treatment completely blocked this effect, indicating that Aβ clearance is dependent on TBK1 pathway activation (Fig. 6C).

Collectively, these in vivo data demonstrate that phenytoin sodium promotes mitophagy by activating TBK1 phosphorylation, thereby facilitating Aβ clearance, maintaining mitochondrial homeostasis, attenuating neuronal apoptosis, and ultimately ameliorating cognitive impairment. TBK1 serves as the core molecular hub for its neuroprotective effects.

4 Discussion

AD, the most prevalent neurodegenerative disorder worldwide, features an extremely complex pathological mechanism. Current therapeutic approaches remain confined to symptomatic relief, and interventions with disease-modifying potential are lacking(Zemek et al., 2014; Cummings, et al., 2016; Zhang, 2021). First-line clinical drugs, such as acetylcholinesterase inhibitors(donepezil, rivastigmine, galantamine)(Brodie, 2017; Rabin et al., 2017) and the NMDA receptor antagonist memantine(Rabin, et al., 2017; Arjmandi-Rad et al., 2024), can only transiently improve cognitive function without halting disease progression(Zemek, et al., 2014; Cummings, et al., 2016). Although progress in reducing cerebral Aβ burden has been achieved with anti-amyloid monoclonal antibodies(Lecanemab, Donanemab) (Melchiorri, et al., 2023; Sims, 2023; Zhang, et al., 2023b), they offer limited overall cognitive benefits and raise safety concerns such as amyloid-related imaging abnormalities(ARIA) (Hardy, 2025). Emerging strategies, including anti-inflammatory therapies(Li et al., 2019; Van Dyck et al., 2023), and stem cell transplantation (Walker and Lue, 2007; Salwa and Kumar, 2021; Honig et al., 2024), remain in the exploratory stage and face a prolonged translational pathway. Therefore, developing disease-modifying therapies with clear mechanisms, controllable safety profiles, and the potential for rapid clinical translation has become a pivotal challenge in AD research.

Mounting evidence indicates that mitochondrial dysfunction is an early driver in the AD pathological cascade(Misrani, et al., 2021; Alqahtani et al., 2023; Narendra and Youle, 2024). Abnormalities such as imbalanced mitochondrial dynamics(Wang et al., 2024b), exacerbated oxidative stress(Misrani, et al., 2021; Leyane, et al., 2022), accumulated mtDNA damage, and disrupted mitochondria–endoplasmic reticulum crosstalk(Atlante A, 2022; Bhatt et al., 2024) are prevalent in the brain tissues of patients with AD and various AD models. These abnormalities not only impair neuronal energy metabolism but also create a vicious cycle

by promoting Aβ deposition and tau hyperphosphorylation. Targeting mitochondrial quality control, particularly the selective activation of mitophagy, has been proven to effectively clear dysfunctional mitochondria, restore mitochondrial homeostasis, and improve neurological function in multiple models(Um and Yun, 2017; Cen X, 2021; Pradeepkiran et al., 2022; Zhou et al., 2023; Han et al., 2024; Sun et al., 2024; Xu, 2024; Zhang et al., 2024). Despite the preclinical potential of inducers such as urolithin A (UA) and UMI-77(Cen et al., 2020a; Cen, et al., 2021a; Zhang, et al., 2024), as well as the exploration of mitochondrial-targeted strategies including MitoQ and resveratrol(Mcmanus, 2011; Cenini and Voos, 2019; Young and Franklin, 2019; Mi et al., 2021; Atlante et al., 2022) , no mitophagy-targeting drug has yet entered clinical validation for AD due to bottlenecks such as low BBB penetration efficiency, insufficient bioavailability, lack of long-term safety data, and high individual pathological heterogeneity(Cen, et al., 2021b; Zhou, et al., 2023; Zhang, et al., 2025a).

Using a drug repositioning strategy, we identified PHT, a classic antiepileptic drug, as a potent mitophagy inducer through high-throughput screening for the first time. In APP/PS1 transgenic mice, long-term low-dose PHT intervention (30 mg·kg−1, oral gavage every other day for 3 months) significantly improved spatial and non-spatial cognitive functions, concurrently reduced hippocampal Aβ1-42 deposition, attenuated neuronal apoptosis, and improved mitochondrial ultrastructural integrity (validated by mt-Keima and TEM). Mechanistically, multidimensional experiments confirmed that PHT promotes the phosphorylation of TBK1 at Ser172. This effect was markedly attenuated both in vitro (TBK1 knockdown/amlexanox inhibition) and in vivo (co-administration of amlexanox/Mdivi-1), accompanied by a loss of behavioral improvement, Aβ clearance, and mitochondrial protection, thereby establishing TBK1 as an indispensable molecular node for the neuroprotective effects of PHT. RNA-seq analysis further revealed (data not shown) that PHT selectively upregulates the autophagic response branch of the cGAS-STING pathway (increased cGAS/STING mRNA expression), rendering cells in a “primed state” that was highly sensitive to mitochondrial damage while avoiding activation of the type I interferon (IFN) inflammatory pathway, presenting a “functional segregation” regulatory feature. This finding provides a molecular basis for PHT as a precise, low-risk autophagy enhancer.

Mitophagy can be mediated through both PINK1/Parkin-dependent and PINK1/Parkin-independent mechanisms. In the present study, the observation that PHT still enhanced TBK1 phosphorylation and promoted TIM23 reduction in HeLa cells suggests that PHT-induced mitochondrial clearance is not strictly dependent on Parkin. However, our additional Western blot results showed that PHT did not further increase total NIX or FUNDC1 protein levels compared with the model group. Therefore, the Parkin-independent effect of PHT may not be explained simply by increased abundance of these receptor-mediated mitophagy proteins. One possibility is that PHT activates TBK1-dependent mitophagy primarily by regulating the activity, phosphorylation, subcellular localization, or protein–protein interactions of downstream autophagy receptors, rather than by increasing their total protein expression. Future studies using receptor knockdown, phosphorylation-site analysis, and mitochondrial recruitment assays are required to identify the precise Parkin-independent downstream machinery involved in PHT-induced mitophagy.

Notably, the established pharmacological actions of PHT—most prominently its use-/frequency-dependent inhibition of voltage-gated sodium channels(D'arcy, 2024) and the consequent suppression of excitatory synaptic transmission, including reduced glutamate release in multiple experimental preparations—can mitigate excitotoxic stress, thereby indirectly attenuating NMDA-driven Ca2+ overload(Pisciotta and Prestipino, 2002; Reddy et al., 2018; Chakravorty et al., 2019; Weissig, 2020). Importantly, this effect is largely indirect rather than a direct antagonism of the NMDA receptor-mediated response (Chakravorty, et al., 2019). In addition, PHT has been reported to modulate other excitability-relevant targets, including the inhibition of L-type Ca2+ currents in certain preparations(Cunningham et al., 2000), effects on voltage-gated K+ currents (Laffling et al., 1995), and the inhibition of AMPA receptor-mediated currents (Bano and Ankarcrona, 2018). Together, these “traditional” actions form a prevention-clearance synergistic loop with the mitochondrial protective mechanism newly identified in this study: PHT alleviates primary mitochondrial injury by dampening excitotoxic stress(Pisciotta and Prestipino, 2002; Reddy, et al., 2018), while also promoting the efficient elimination of damaged mitochondria via TBK1-dependent mitoph-

agy, preserving ΔΨm homeostasis, and supporting effective autophagic turnover by maintaining a healthier mitochondrial pool(Cen, et al., 2020a; Cen, et al., 2021a). This dual mechanism is distinct from single-pathway intervention strategies and further broadens the therapeutic scope of PHT in neurodegenerative diseases(Mi, et al., 2021; Atlante, et al., 2022).

PHT exhibits prominent clinical translational advantages over existing mitophagy inducers. UA can activate mitophagy; however, in humans, systemic exposure to the parent aglycone is typically in the nanomolar range following oral administration, and UA is predominantly detected as glucuronide/sulfate conjugates, consistent with substantial first-pass metabolism(Dron et al., 2021; Zhang et al., 2025b). UA also antagonizes aryl hydrocarbon receptor (AhR) signaling. In competitive binding assays, the IC50 is approximately 0.8–1 μM, whereas functional cell-based reporter assays often yield IC50 values in the low-micromolar range, depending on the inducer and assay context(Muku et al., 2018). Given the role of AhR in mucosal and immune homeostasis, the potential immunological implications of AhR antagonism warrant further evaluation in the intended population and dosing range. In addition, some in vitro systems suggest that UA and related urolithins may exhibit condition-dependent pro-oxidant effects at high concentrations(Kallio et al., 2013), highlighting the need to consider oxidative stress risk under high-exposure scenarios. Animal studies indicate that UA can reach brain tissue, but central exposure is substantially lower than peripheral exposure(Zhang, et al., 2025b).

NAD+ precursors generally act via metabolic conversion and downstream metabolic remodeling; however, achieving a stable shift in peripheral metabolic profiles typically requires repeated dosing over several days to approximately 2 weeks, and tissue distribution can be heterogeneous. Long-term safety at high doses should be interpreted compound-, dose-, and population-specifically, with systematic monitoring for metabolism-related adverse outcomes(Mira and Cerpa, 2021).

In contrast, PHT, a long-marketed classic drug, is supported by a comparatively comprehensive safety evidence base; it exhibits high oral bioavailability (≈90%) and can access the central nervous system(Rivet et al., 1990; Andreux, et al., 2019; D'arcy, 2024). In our study, long-term low-dose PHT treatment in APP/PS1 mice did not elicit typical adverse reactions such as ataxia or arrhythmia, suggesting good tolerability within the tested dose range. Importantly, as an approved drug, PHT may, after appropriate regulatory interaction, leverage existing safety information through pathways such as FDA 505(b)(2) to reduce redundant early-stage development burden; nevertheless, necessary bridging and clinical verification are required for the new indication, dosing, and target population before advancing to exploratory clinical trials(Zhou, et al., 2023; Zhang, et al., 2025b).

Despite the promising neuroprotective effects of PHT identified in this study, several limitations warrant consideration. First, while PHT significantly improved both mitochondrial and cognitive metrics, it did not achieve complete phenotypic rescue; for instance, the recovery of mitochondrial membrane potential (Δψm) in vitro and the reduction of escape latency in the Barnes maze in vivo were distinct but remained partial compared with healthy controls. Second, our in vivo findings rely heavily on the APP/PS1 transgenic mouse model. While this model robustly mimics Aβ-driven pathology, it does not fully capture tau hyperphosphorylation or neurofibrillary tangle formation, which are also central features of human AD. Third, only male APP/PS1 mice were used in this study, and future studies including female mice are needed to assess whether the therapeutic effects of PHT are sex-dependent(Kong et al., 2026). Fourth, while PHT increased TBK1 Ser172 phosphorylation, the present study does not prove direct binding between PHT and TBK1 or its upstream regulators. PHT may activate the TBK1-centered mitophagy cascade indirectly by modulating mitochondrial stress signals, calcium homeostasis, ROS production, or upstream damage-sensing pathways. Finally, although long-term low-dose PHT treatment did not elicit typical adverse reactions such as ataxia or arrhythmia in our mouse study, clinical translation for chronic use in elderly populations requires careful safety monitoring and human validation.

Collectively, these results suggest that PHT promotes TBK1-centered mitophagy, contributing to a cascade protective effect involving the attenuation of primary damage, the clearance of dysfunctional mitochon-

dria, and the improvement of AD-related pathology (Fig. 7). This finding not only provides a theoretical basis and translational pathway for drug repurposing but also supports TBK1-mediated mitophagy as a potential targeting dimension for disease-modifying AD therapy.

Data availability statement

All data in this study are available within the paper and its Supplementary Information.

Acknowledgements

The present study was supported by funding from the National Key Research and Development Program of China (2023YFC2506200)；(2023YFC2506203) ,the National Key Research and Development Program of China (No. 2025YFF1500400), the Natural Science Foundation of Zhejiang Province (No. RG26C070001), the Leading Innovative and Entrepreneur Team Introduction Program of Zhejiang, China (No. 2023TD1061), the Hangzhou Municipal Key Research Program, China (No. 2025SZD1B12), and the Qingke Project of the Zhejiang Provincial Natural Science Foundation (No. LQK26C070002).

Author contributions

Z.C. and X.C. contributed equally to this work. Z.C. conducted the experiments, analyzed the data, and drafted the manuscript. X.C. participated in study design, data analysis, and manuscript revision. F.W., J.Z., Y.T., and M.Z. contributed to experimental assistance, data collection, and result interpretation. J.W., L.X., X.X., and H.X. conceived the study, supervised the project, revised the manuscript critically for important intellectual content, and provided funding support. All authors read and approved the final manuscript and agree to be accountable for all aspects of the work.

Compliance with ethics guidelines

No conflicts of interest, financial or otherwise, are declared by the authors. All procedures followed were in accordance with the ethical standards of the responsible committee on human experimentation (institutional and national) and with the Helsinki Declaration of 1975, as revised in 2008(5). Informed consent was obtained from all patients included in the study. Additional informed consent was obtained from all patients for whom identifying information is included in this article.

Declaration on the Use of Generative AI Tools

During the preparation of this manuscript, the authors used generative AI tools, including ChatGPT, Gemini, and Doubao, solely for language polishing, readability improvement, and minor stylistic suggestions. These tools were not used to generate scientific content, interpret data, perform analyses, or draft the substantive text of the manuscript. After using these tools, the authors carefully reviewed, edited, and verified all content as needed and take full responsibility for the accuracy, integrity, and clarity of the publication.

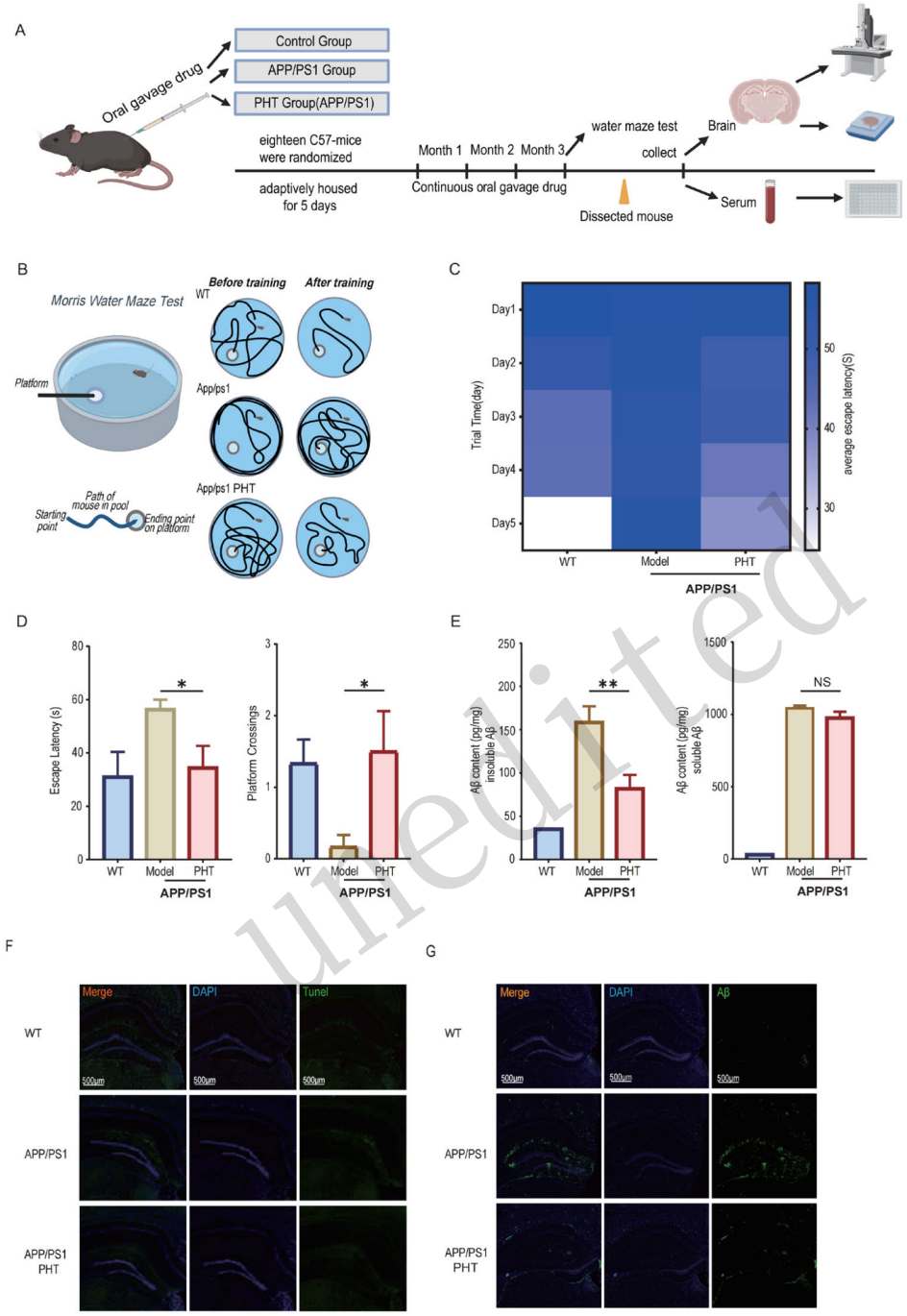

Fig. 1 PHT intervention improves spatial learning and memory and alleviates pathological alterations in APP/PS1 mice.

(A) Schematic diagram of animal model establishment and experimental sample collection.

(B) Schematic illustration of the Morris water maze test and representative swimming trajectories (before/after training).

(C) Heatmap showing the average escape latency during the 5-day training period in each group (N = 6).

(D) Escape latency and platform crossing times on the probe test day after 5 days of training (N = 6).

(E) Comparison of Aβ content (pg/mg) in hippocampal tissues of mice (N = 6).

(F) Representative TUNEL staining images (merge/DAPI/TUNEL) in the hippocampus showing neuronal apoptosis (scale bar as indicated).

(G) Representative immunofluorescence images (merge/DAPI/Aβ) in the hippocampus showing astrocyte activation and Aβ deposition (scale bar as indicated).

Data were analyzed using the unpaired Student's t-test. ** $P < 0.05$;** $P < 0.01$; ns, not significant.

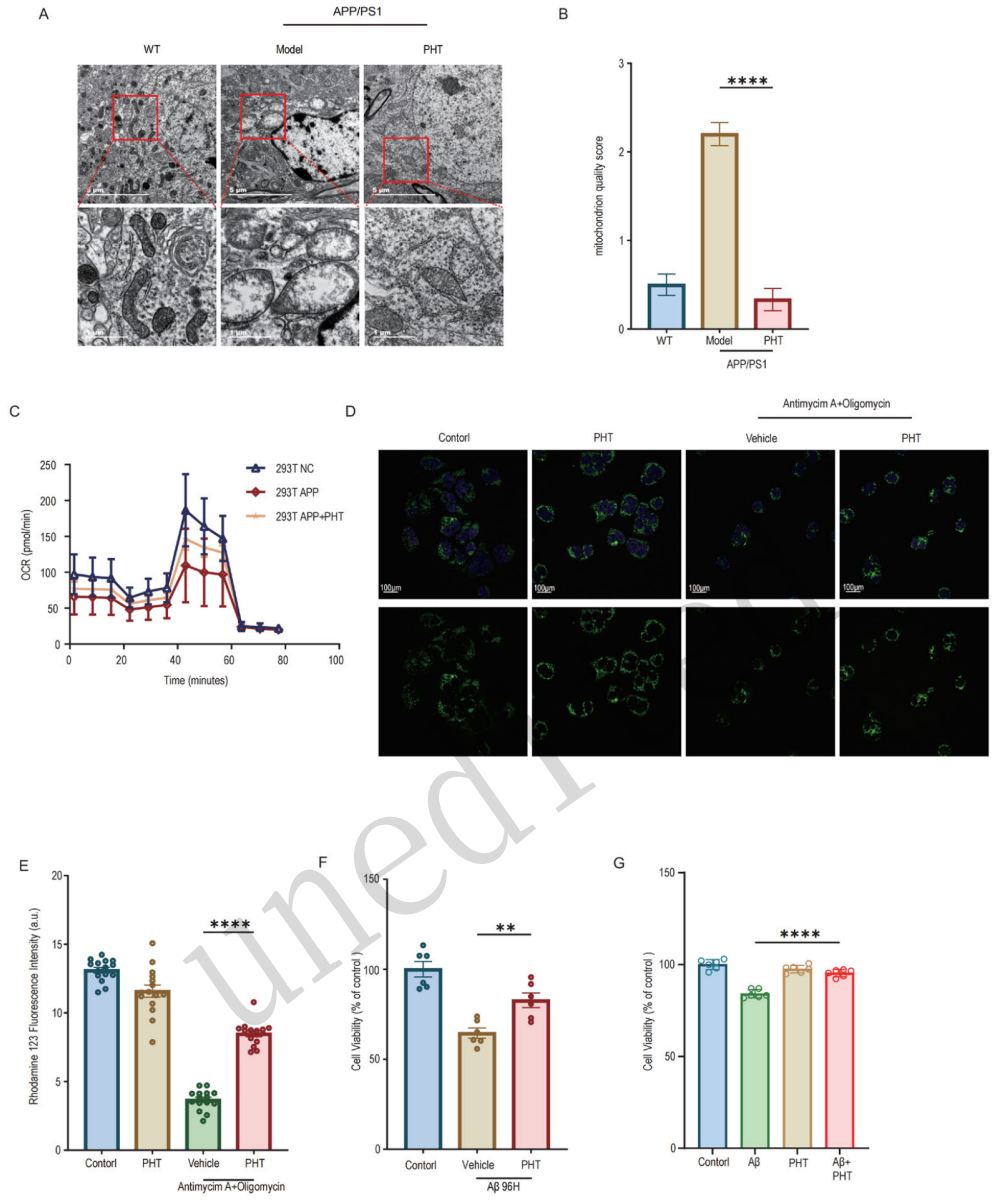

Fig. 2 PHT improves mitochondrial function and enhances cell viability in the APP/PS1 model.

(A) Transmission electron microscopy images of hippocampal (or cortical) tissues from APP/PS1 mice showing the mitochondrial ultrastructure in WT, model, and PHT-treated groups; boxed areas are magnified views.

(B) Quantification of mitochondrial quality scores (N = 20–31 mitochondria/group).

(C) Seahorse analysis showing oxygen consumption rate (OCR) over time in 293T cells under control (NC), APP overexpression, and APP + PHT conditions (N = 6).

(D) Rhodamine 123 staining to assess mitochondrial membrane potential: representative fluorescence images under control/vehicle and PHT

treatment, as well as antimycin A + oligomycin treatment.

(E) Quantification of rhodamine 123 fluorescence intensity. Statistical significance is indicated by asterisks (each point represents one cell; N = 15 cells).

(F) Comparison of cell viability in SH-SY5Y cells after 96 h of Aβ stimulation under vehicle and PHT treatment (each point represents one well of a 96-well plate, with N = 6 wells).

(G) Comparison of cell viability in SH-SY5Y cells under control, Aβ, PHT, and Aβ + PHT treatment conditions (each point represents one well of a 96-well plate, with N = 6 wells).

Data were analyzed using the unpaired Student's t-test. ** $P < 0.01$; **** $P < 0.0001$

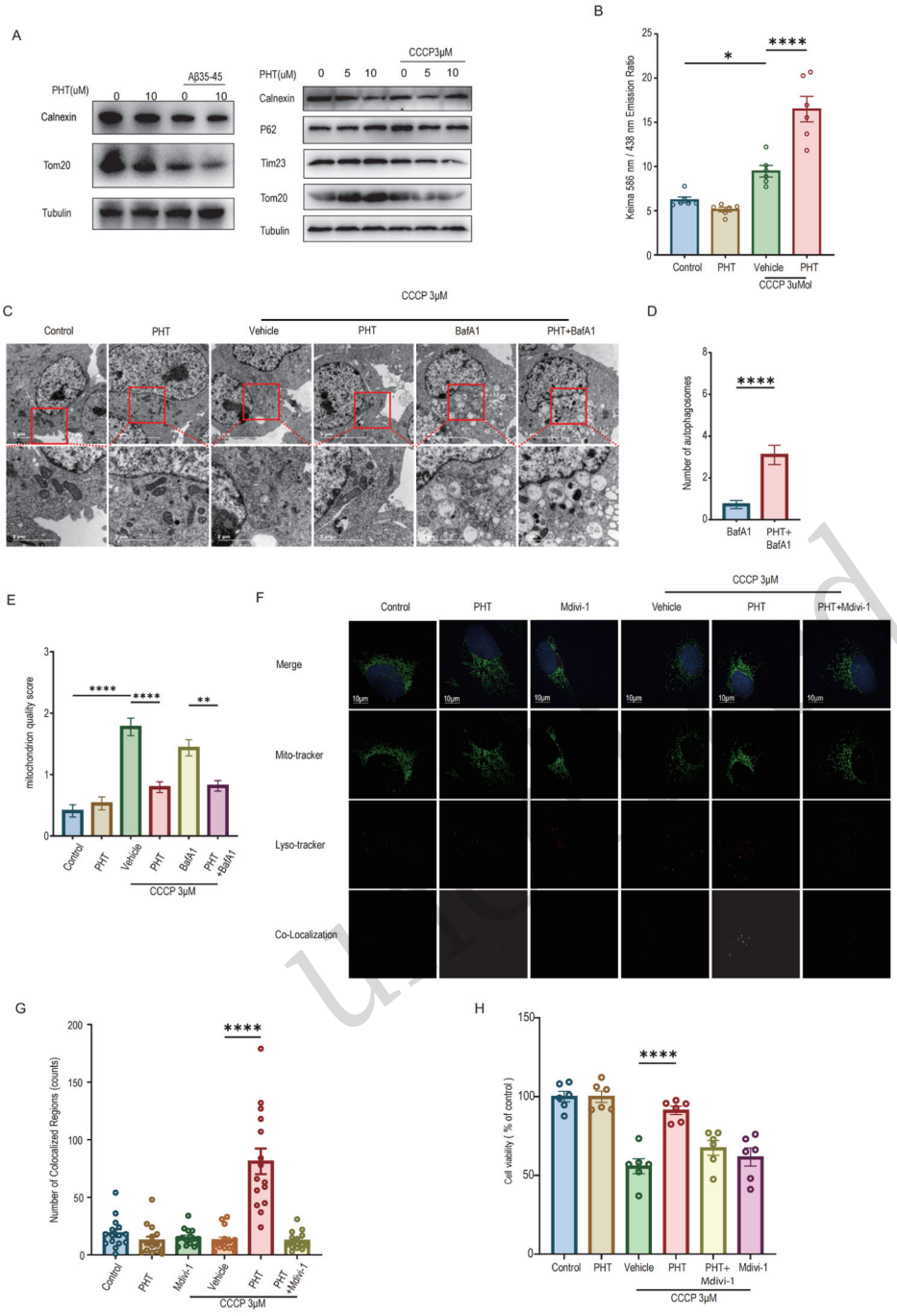

Fig. 3 PHT promotes clearance of damaged mitochondria and improves mitochondrial quality (CCCP-induced model).

(A) Immunoblot analysis of related proteins in SH-SY5Y cells under Aβ and CCCP stimulation with different treatments (including Mdivi-1 combination).

(B) mt-Keima assay showing mitophagy levels in HEK293T-mito-Keima cells; the Keima 586/438 nm emission ratio reflects the extent of mitochondria delivered to lysosomes (each point represents one well of a 96-well plate, with N = 6 wells).

(C) Transmission electron microscopy images showing the mitochondrial ultrastructure and autophagy-related changes under different treatments in SH-SY5Y cells (including BafA1).

(D) Quantification of autophagosome numbers (BafA1 vs. PHT + BafA1; N = 6).

(E) Quantification of mitochondrial quality scores (N = 22–35 mitochondria/group).

(F) MitoTracker and LysoTracker co-localization imaging and quantification of co-localized regions in U2OS cells.

(G) Statistical analysis of co-localization counts is shown in (F) (each point represents one cell; N = 15 cells).

(H) Effects of different treatments (PHT, Mdivi-1, and combination) on cell viability in SH-SY5Y cells under CCCP (3 μM) induction (each point represents one well of a 96-well plate, with N = 6 wells).

(D)(G)(H) Data were analyzed using the unpaired Student's t-test. **** $P < 0.0001$

(B)(E) Data were analyzed using one-way ANOVA. * $P < 0.05$； ** $P < 0.01$； **** $P < 0.0001$

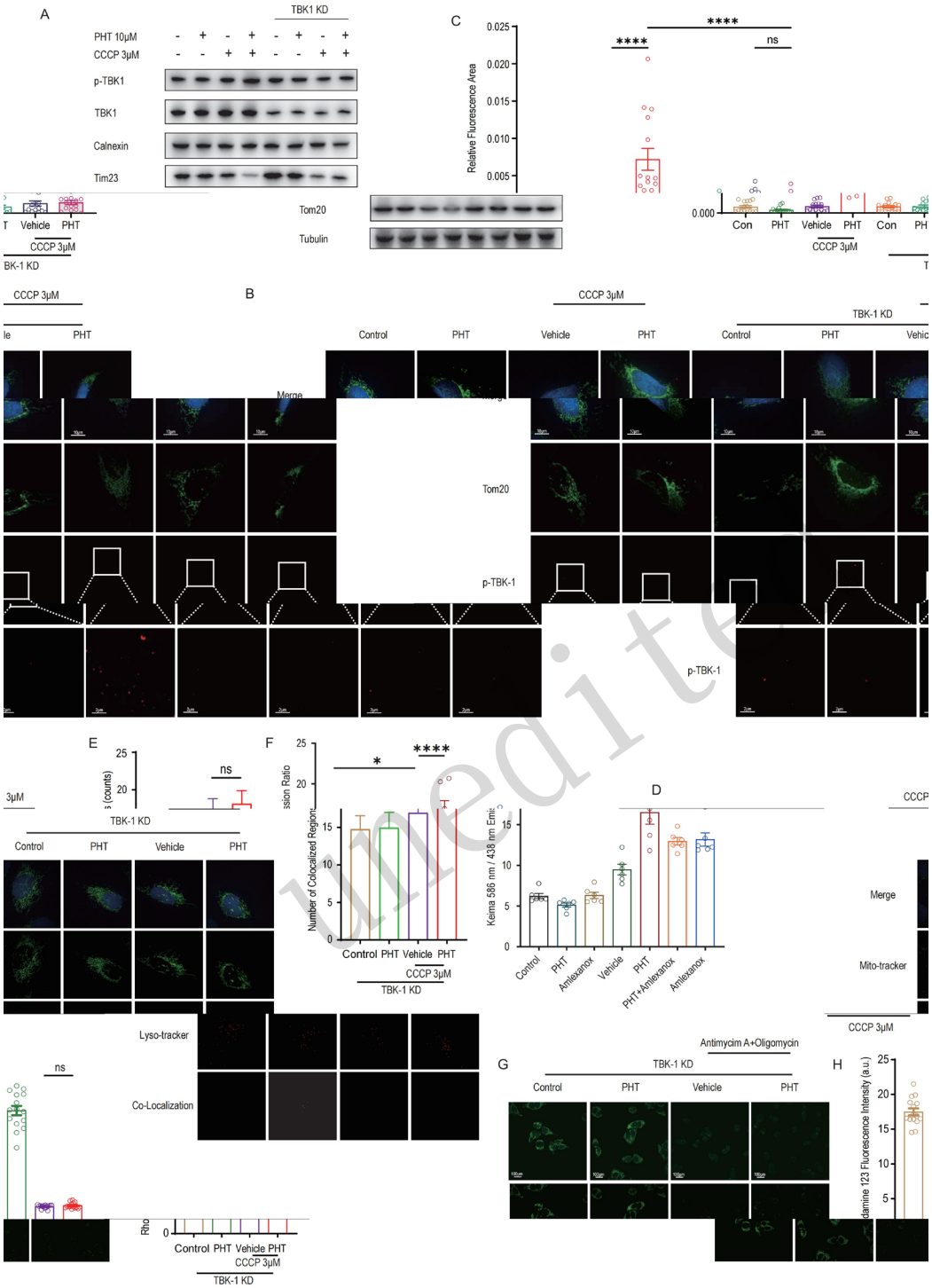
A
TBK1 KD
PHT 10μM
CCCP 3μM
p-TBK1
TBK1
Calnexin
Tim23
Tom20
Tubulin
Vehicle
PHT
CCCP 3μM
C
Relative Fluorescence Area
****
ns
Con
PHT
Vehicle
PHT
Con
PH
B
CCCP 3μM
TBK-1 KD
Control
PHT
Vehicle
Merge
Tom20
p-TBK-1
E
ns
TBK-1 KD
F
Number of Colocalized Regions
*
****
D
Keima 586 nm / 438 nm Emi
Control
PHT
Amlexanox
Vehicle
PHT+Amlexanox
Mito-tracker
Lyso-tracker
Co-Localization
G
Antimycin A+Oligomycin
H
Rhodamine 123 Fluorescence Intensity (a.u.)

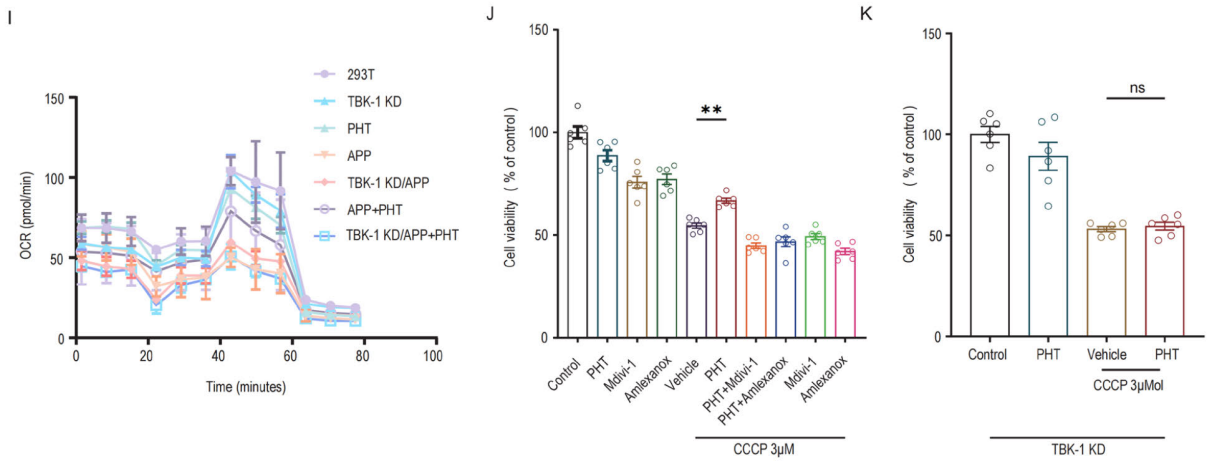

Fig. 4 TBK1 knockdown attenuates the protective effects of PHT on mitochondrial quality control and mitophagy.

(A) Immunoblot analysis of p-TBK1, TBK1, and mitochondrial-related proteins in SH-SY5Y TBK1 knockdown (KD) cells treated with PHT (10 μM) and CCCP (3 μM).

(B) MitoTracker and LysoTracker co-localization imaging and quantification of co-localized regions in U2OS cells.

(C) Statistical analysis of co-localization counts shown in (B) (each point represents one cell; N = 15 cells).

(D) Immunofluorescence staining of Tom20 and p-TBK1 showing the spatial relationship between TBK1 activation and mitochondrial markers in U2OS cells; boxed areas indicate magnified views.

(E) Quantification of related fluorescence area/signals. Asterisks indicate statistical significance; ns indicates no significant difference.

(F) mt-Keima assay (Keima 586/438 ratio) showing the regulation of mitophagy levels by PHT and combination with amlexanox in HEK293T-mito-Keima cells under CCCP induction (each point represents one well of a 96-well plate, with N = 6 wells).

(G) Representative images of mitochondrial membrane potential assessed by rhodamine 123 staining in TBK1 KD 293T cells under antimycin A + oligomycin treatment.

(H) Quantification of rhodamine 123 fluorescence intensity (each point represents one cell; N = 15 cells).

(I) Seahorse analysis showing OCR curves in 293T and 293T-TBK1 KD cells under APP overexpression and PHT treatment (each point represents one well of a 96-well plate, with N = 6 wells).

(J) Effects of different treatments (PHT, Mdivi-1, amlexanox, and combinations) on cell viability in SH-SY5Y cells under CCCP (3 μM) induction (each point represents one well of a 96-well plate, with N = 6 wells).

(K) Effects of different treatments on CCCP-induced cell viability in the SHSY5Y-TBK1 KD background (each point represents one well of a 96-well plate, with N = 6 wells).

Data were analyzed using one-way ANOVA. * $P < 0.05$; ** $P < 0.01$; **** $P < 0.0001$; ns, not significant.

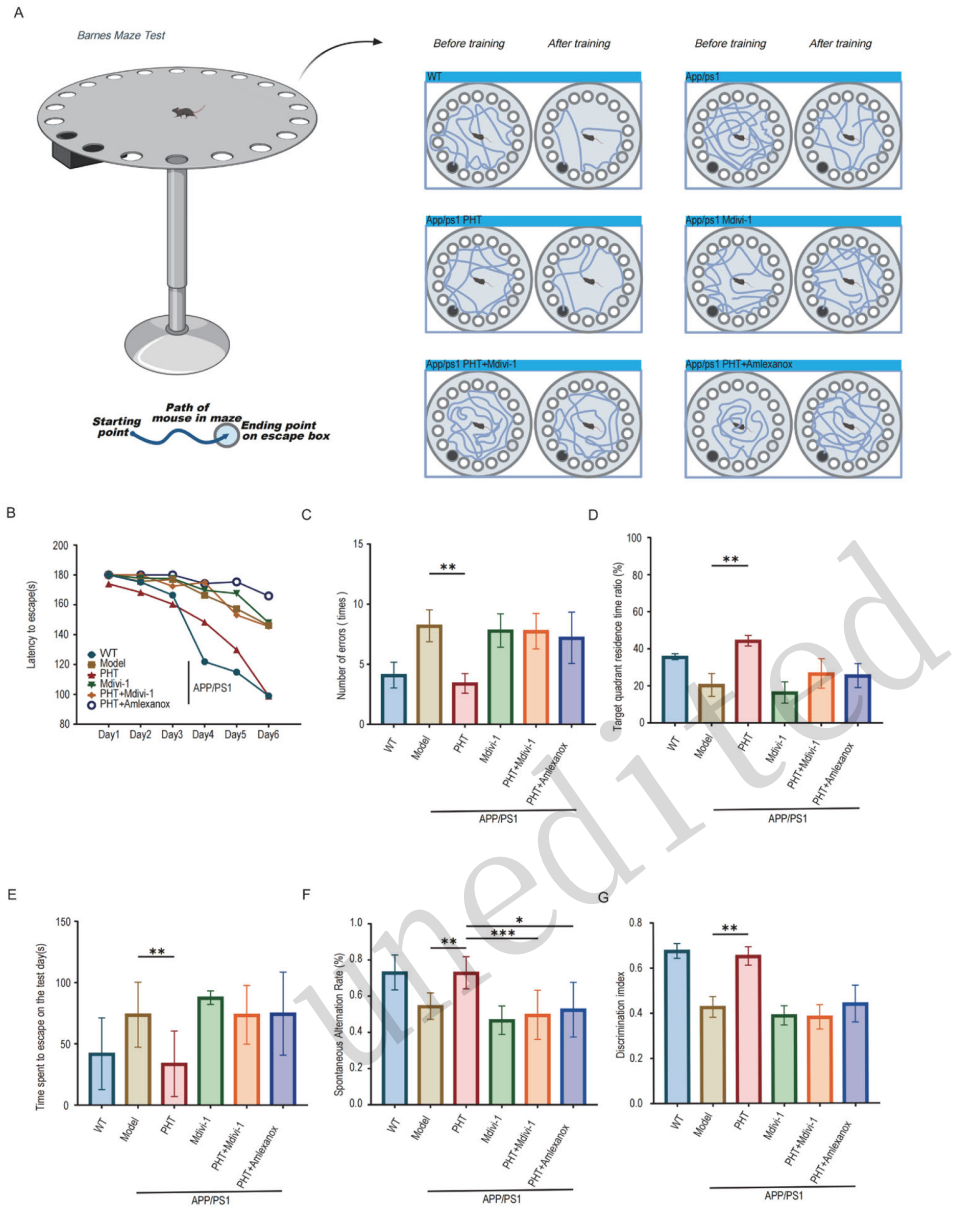

Fig. 5 PHT and combination treatments alter learning, memory, and cognitive behaviors in APP/PS1 mice.

(A) Schematic diagram of the Barnes maze and representative trajectories (before training/after training).

(B) Escape latency during Barnes maze training days (days 1–6; N = 6–10 mice/group).

(C) Number of errors on the test day in the Barnes maze (N = 6–10 mice/group).

(D) Percentage of time spent in the target quadrant on the test day (N = 6–10 mice/group).

(E) Time required to reach the escape hole on the test day (N = 6–10 mice/group).

(F) Spontaneous alternation rate in the Y-maze (N = 6–10 mice/group).

(G) Discrimination index in the novel object recognition test (N = 6–10 mice/group).

Data were analyzed using one-way ANOVA. * $P < 0.05$； ** $P < 0.01$； *** $P < 0.001$

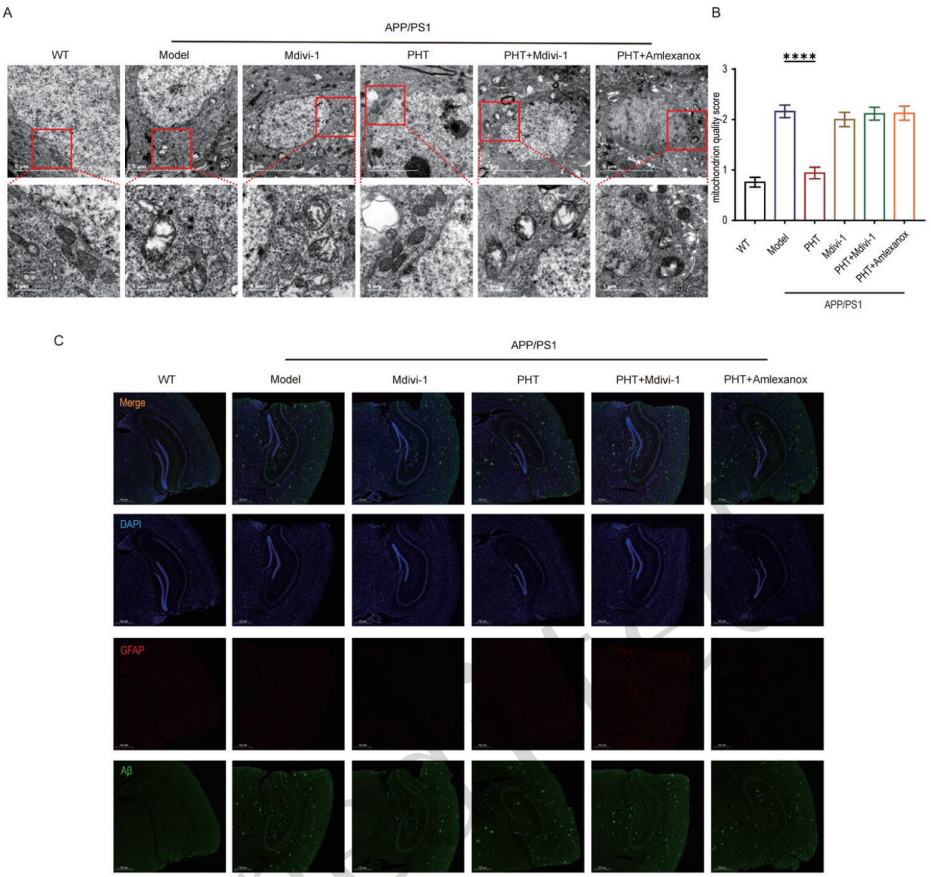

Fig. 6 Inhibition of the TBK1 pathway or mitophagy attenuates the protective effects of PHT.

(A) Transmission electron microscopy images and magnified views of mitochondrial morphology in different treatment groups of APP/PS1 mice (WT, model, Mdivi-1, PHT, PHT + Mdivi-1, PHT + amlexanox).

(B) Quantification of mitochondrial quality scores (N = 20–35 mitochondria/group).

(C) Immunofluorescence staining of brain tissues (DAPI, GFAP, and Aβ) showing the effects of different treatments on astrocytic responses and Aβ deposition.

Data were analyzed using the unpaired Student's t-test. ****P < 0.0001

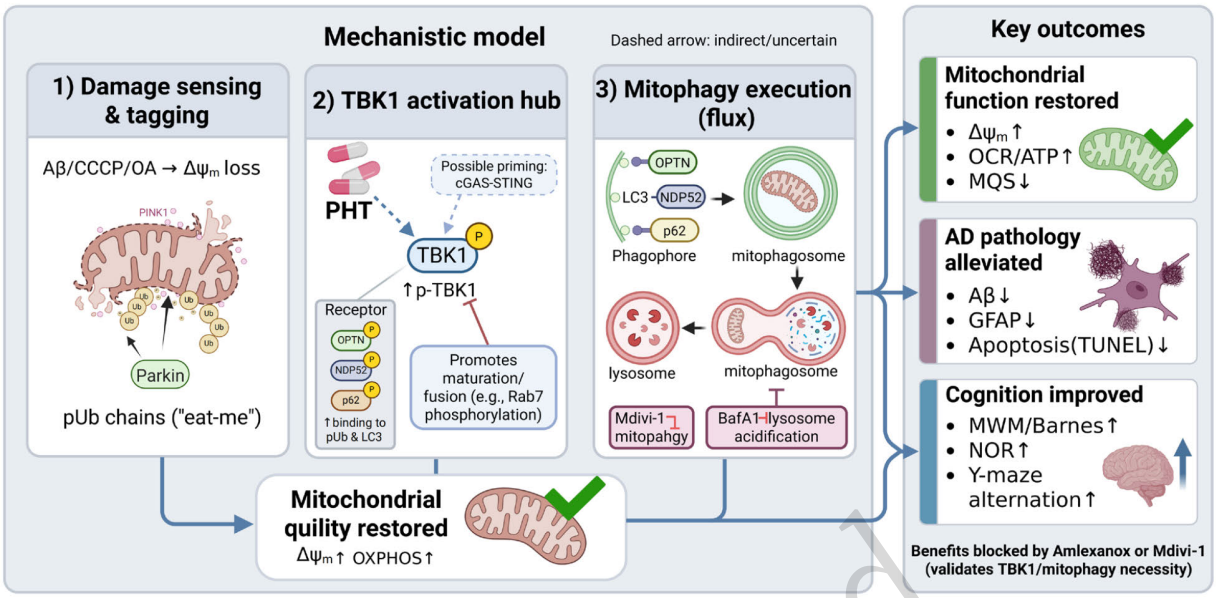

Fig. 7 Proposed schematic model illustrating the mechanism by which PHT activates the TBK1 pathway to enhance mitophagy, improve mitochondrial quality control, and ultimately ameliorate cognitive dysfunction in APP/PS1 mice.

References

Agrawal I JS, 2020. Mitochondrial dysfunction and alzheimer's disease: Role of microglia. *Front Aging Neurosci*, 12:252.

Alqahtani T, Deore SL, Kide AA, et al., 2023. Mitochondrial dysfunction and oxidative stress in alzheimer's disease, and parkinson's disease, huntington's disease and amyotrophic lateral sclerosis -an updated review. *Mitochondrion*, 71:83-92. https://doi.org/10.1016/j.mito.2023.05.007

Andreux PA, Blanco-Bose W, Ryu D, et al., 2019. The mitophagy activator urolithin a is safe and induces a molecular signature of improved mitochondrial and cellular health in humans. *Nat Metab*, 1(6):595-603. https://doi.org/10.1038/s42255-019-0073-4

Arjmandi-Rad S, Vestergaard Nieland JD, Goozee KG, et al., 2024. The effects of different acetylcholinesterase inhibitors on eeg patterns in patients with alzheimer's disease: A systematic review. *Neurol Sci*, 45(2):417-430. https://doi.org/10.1007/s10072-023-07114-y

Ashleigh T, Swerdlow RH, Beal MF, 2023. The role of mitochondrial dysfunction in alzheimer's disease pathogenesis. *Alzheimers Dement*, 19(1):333-342. https://doi.org/10.1002/alz.12683

Atlante A, Amadoro G, Latina V, 2022. Therapeutic potential of targeting mitochondria for alzheimer's disease treatment. *J Clin Med*, 11(22):6742.

Atlante A VD, Latina V, Amadoro G., 2022. Dysfunction of mitochondria in alzheimer's disease: Ant and vdac interact with toxic proteins and aid to determine the fate of brain cells. *Int J Mol Sci*, 23(14):7722.

Bano D, Ankarcrona M, 2018. Beyond the critical point: An overview of excitotoxicity, calcium overload and the downstream consequences. *Neurosci Lett*, 663:79-85.

Bhatt A, Bhardwaj H, Srivastava P, 2024. Mesenchymal stem cell therapy for alzheimer's disease: A novel therapeutic approach for neurodegenerative diseases. *Neuroscience*, 555:52-68.

Bourdenx M, Martín-Segura A, Scrivo A, et al., 2021. Chaperone-mediated autophagy prevents collapse of the neuronal metastable proteome. *Cell*, 184(10):2696-2714.e2625. https://doi.org/10.1016/j.cell.2021.03.048

Brodie MJ, 2017. Sodium channel blockers in the treatment of epilepsy. *CNS Drugs*, 31(7):527-534.

Cen X, Chen Y, Xu X, 2020a. Pharmacological targeting of mcl-1 promotes mitophagy and improves disease pathologies in an alzheimer's disease mouse model. *Nat Commun*, 11(1):5731.

Cen X, Chen Y, Xu X, et al., 2020b. Pharmacological targeting of mcl-1 promotes mitophagy and improves disease pathologies in an alzheimer's disease mouse model. *Nat Commun*, 11(1):5731. https://doi.org/10.1038/s41467-020-19547-6

Cen X, Xu X, Xia H, 2021a. Targeting mcl1 to induce mitophagy is a potential therapeutic strategy for alzheimer disease. *Autophagy*, 17(3):818-819. https://doi.org/10.1080/15548627.2020.1860542

Cen X, Zhang M, Zhou M, et al., 2021b. Mitophagy regulates neurodegenerative diseases. *Cells*, 10(8) https://doi.org/10.3390/cells10081876

Cen X CY, Xu X, Wu R, He F, Zhao Q, Sun Q, Yi C, Wu J, Najafov a, Xia H. , 2020. Pharmacological targeting of mcl-1 promotes mitophagy and improves disease pathologies in an alzheimer's disease mouse model. *Nat Commun*, 11(1):5731.

Cen X XX, Xia H. , 2021. Targeting mcl1 to induce mitophagy is a potential therapeutic strategy for alzheimer disease. *Autophagy*, 17(3):818-819.

Cenini G, Voos W, 2019. Mitochondria as potential targets in alzheimer disease therapy: An update. *Front Pharmacol*, 10:902.

Chakravorty A, Jetto CT, Manjithaya R, 2019. Dysfunctional mitochondria and mitophagy as drivers of alzheimer's disease pathogenesis. *Front Aging Neurosci*, 11:311.

Cummings J, Aisen PS, Dubois B, et al., 2016. Drug development in alzheimer's disease: The path to 2025. *Alzheimers Res Ther*, 8:39. https://doi.org/10.1186/s13195-016-0207-9

Cunningham MO, Dhillon A, Wood SJ, et al., 2000. Reciprocal modulation of glutamate and gaba release may underlie the anticonvulsant effect of phenytoin. *Neuroscience*, 95(2):343-351. https://doi.org/10.1016/s0306-4522(99)00468-6

D'arcy MS, 2024. Mitophagy in health and disease. Molecular mechanisms, regulatory pathways, and therapeutic implications. *Apoptosis*, 29(9-10):1415-1428.

Dron MY, Zhigulin AS, Tikhonov DB, et al., 2021. Screening for activity against ampa receptors among anticon-

vulsants-focus on phenytoin. *Front Pharmacol*, 12:775040. https://doi.org/10.3389/fphar.2021.775040

Han Z, Wang B, Wen YQ, et al., 2024. Acteoside alleviates lipid peroxidation by enhancing nrf2-mediated mitophagy to inhibit ferroptosis for neuroprotection in parkinson's disease. *Free Radic Biol Med*, 223:493-505. https://doi.org/10.1016/j.freeradbiomed.2024.07.018

Hardy J, 2025. Alzheimer's disease: Treatment challenges for the future. *J Neurochem*, 169(8):e70176. https://doi.org/10.1111/jnc.70176

Heo JM, Ordureau A, Paulo JA, et al., 2015. The pink1-parkin mitochondrial ubiquitylation pathway drives a program of optn/ndp52 recruitment and tbk1 activation to promote mitophagy. *Mol Cell*, 60(1):7-20. https://doi.org/10.1016/j.molcel.2015.08.016

Honig LS, Sabbagh MN, Van Dyck CH, et al., 2024. Updated safety results from phase 3 lecanemab study in early alzheimer's disease. *Alzheimers Res Ther*, 16(1):105. https://doi.org/10.1186/s13195-024-01441-8

Ising C, Venegas C, Zhang S, et al., 2019. Nlrp3 inflammasome activation drives tau pathology. *Nature*, 575(7784):669-673. https://doi.org/10.1038/s41586-019-1769-z

Kallio T, Kallio J, Jaakkola M, et al., 2013. Urolithins display both antioxidant and pro-oxidant activities depending on assay system and conditions. *J Agric Food Chem*, 61(45):10720-10729. https://doi.org/10.1021/jf403208d

Kataura T, Otten EG, Rabanal-Ruiz Y, et al., 2023. Ndp52 acts as a redox sensor in pink1/parkin-mediated mitophagy. *Embo j*, 42(5):e111372. https://doi.org/10.15252/embj.2022111372

Kong L, Yang Y, Zhou W, et al., 2026. Sporadic alzheimer's disease with bipolar-like features: A case report and a brief review of the current research status. *J Zhejiang Univ Sci B*, 27(4):416-425. https://doi.org/10.1631/jzus.B2500307

Laffling AJ, Scherr P, Mcgivern JG, et al., 1995. Electrophysiological actions of phenytoin on n-methyl-d-aspartate receptor-mediated responses in rat hippocampus in vitro. *Br J Pharmacol*, 115(1):67-72. https://doi.org/10.1111/j.1476-5381.1995.tb16320.x

Lau V, Ramer L, Tremblay M, 2023. An aging, pathology burden, and glial senescence build-up hypothesis for late onset alzheimer's disease. *Nat Commun*, 14(1):1670. https://doi.org/10.1038/s41467-023-37304-3

Lazarou M SD, Kane La, Sarraf Sa, Wang C, Burman Jl, Sideris Dp, Fogel Ai, Youle Rj. , 2015. The ubiquitin kinase pink1 recruits autophagy receptors to induce mitophagy. *Nature*, 524(7565):309-314.

Leyane TS, Jere SW, Houreld NN, 2022. Oxidative stress in ageing and chronic degenerative pathologies: Molecular mechanisms involved in counteracting oxidative stress and chronic inflammation. *Int J Mol Sci*, 23(13) https://doi.org/10.3390/ijms23137273

Li DD, Zhang YH, Zhang W, et al., 2019. Meta-analysis of randomized controlled trials on the efficacy and safety of donepezil, galantamine, rivastigmine, and memantine for the treatment of alzheimer's disease. *Front Neurosci*, 13:472. https://doi.org/10.3389/fnins.2019.00472

Li J, Lai M, Zhang X, et al., 2022. Pink1-parkin-mediated neuronal mitophagy deficiency in prion disease. *Cell Death Dis*, 13(2):162. https://doi.org/10.1038/s41419-022-04613-2

Liu N, Luo K, Yuan Z, et al., 2022. A transfer learning method for detecting alzheimer's disease based on speech and natural language processing. *Front Public Health*, 10:772592. https://doi.org/10.3389/fpubh.2022.772592

Maeda S, Yamamoto H, Kinch LN, et al., 2020. Structure, lipid scrambling activity and role in autophagosome formation of atg9a. *Nat Struct Mol Biol*, 27(12):1194-1201. https://doi.org/10.1038/s41594-020-00520-2

Marinković M, Šprung M, Novak I, 2021. Dimerization of mitophagy receptor bnip3l/nix is essential for recruitment of autophagic machinery. *Autophagy*, 17(5):1232-1243. https://doi.org/10.1080/15548627.2020.1755120

Mary A, Eysert F, Checler F, et al., 2023. Mitophagy in alzheimer's disease: Molecular defects and therapeutic approaches. *Mol Psychiatry*, 28(1):202-216. https://doi.org/10.1038/s41380-022-01631-6

Mcmanus MJ, 2011. The mitochondria-targeted antioxidant mitoq prevents loss of spatial memory retention and early neuropathology in a transgenic mouse model of alzheimer's disease. *J Neurosci*, 31(44):15703-15715.

Melchiorri D, Merlo S, Micallef B, et al., 2023. Alzheimer's disease and neuroinflammation: Will new drugs in clinical trials pave the way to a multi-target therapy? *Front Pharmacol*, 14:1196413. https://doi.org/10.3389/fphar.2023.1196413

Mi Y, Qi G, Brinton RD, et al., 2021. Mitochondria-targeted therapeutics for alzheimer's disease: The good, the bad, the potential. *Antioxid Redox Signal*, 34(8):611-630. https://doi.org/10.1089/ars.2020.8070

Mira RG, Cerpa W, 2021. Building a bridge between nmdar-mediated excitotoxicity and mitochondrial dysfunction in chronic and acute diseases. *Cell Mol Neurobiol*, 41(7):1413-1430.

Misrani A, Tabassum S, Yang L, 2021. Mitochondrial dysfunction and oxidative stress in alzheimer's disease. *Front Aging Neurosci*, 13:617588.

Muku GE, Murray IA, Espín JC, et al., 2018. Urolithin a is a dietary microbiota-derived human aryl hydrocarbon receptor antagonist. *Metabolites*, 8(4) https://doi.org/10.3390/metabo8040086

Narendra DP, Youle RJ, 2024. The role of pink1–parkin in mitochondrial quality control. *Nature Cell Biology*, 26(10):1639-1651.

Narendra Dp YR, 2024. The role of pink1–parkin in mitochondrial quality control. *Nature Cell Biology*, 26(10):1639-1651.

Palmqvist S, Tideman P, Cullen N, et al., 2021. Prediction of future alzheimer's disease dementia using plasma phospho-tau combined with other accessible measures. *Nat Med*, 27(6):1034-1042. https://doi.org/10.1038/s41591-021-01348-z

Pickrell AM, Youle RJ, 2015. The roles of pink1, parkin, and mitochondrial fidelity in parkinson's disease. *Neuron*, 85(2):257-273.

Pisciotta M, Prestipino G, 2002. Anticonvulsant phenytoin affects voltage-gated potassium currents in cerebellar granule cells. *Brain Res*, 941(1-2):53-61.

Pradeepkiran JA, Hindle A, Kshirsagar S, et al., 2022. Are mitophagy enhancers therapeutic targets for alzheimer's disease? *Biomed Pharmacother*, 149:112918. https://doi.org/10.1016/j.biopha.2022.112918

Rabin LA, Smart CM, Amariglio RE, 2017. Subjective cognitive decline in preclinical alzheimer's disease. *Annu Rev Clin Psychol*, 13:369-396.

Reddy PH, Yin X, Manczak M, et al., 2018. Mutant app and amyloid beta-induced defective autophagy, mitophagy, mitochondrial structural and functional changes and synaptic damage in hippocampal neurons from alzheimer's disease. *Hum Mol Genet*, 27(14):2502-2516. https://doi.org/10.1093/hmg/ddy154

Rivet M, Bois P, Cognard C, et al., 1990. Phenytoin preferentially inhibits l-type calcium currents in whole-cell patch-clamped cardiac and skeletal muscle cells. *Cell Calcium*, 11(9):581-588. https://doi.org/10.1016/0143-4160(90)90012-j

Rizzo MG, De Plano LM, Palermo N, et al., 2023. A novel serum-based diagnosis of alzheimer's disease using an advanced phage-based biochip. *Adv Sci (Weinh)*, 10(21):e2301650. https://doi.org/10.1002/advs.202301650

Roda AR, Serra-Mir G, Montoliu-Gaya L, et al., 2022. Amyloid-beta peptide and tau protein crosstalk in alzheimer's disease. *Neural Regen Res*, 17(8):1666-1674. https://doi.org/10.4103/1673-5374.332127

Salwa, Kumar L, 2021. Engrafted stem cell therapy for alzheimer's disease: A promising treatment strategy with clinical outcome. *J Control Release*, 338:837-857.

Sehar U, Priyanka Rawat, Arubala P. Reddy, et al., 2022. U., et al., amyloid beta in aging and alzheimer's disease. *International Journal of Molecular Sciences*, 23(21):12924.

Sims JR, 2023. Donanemab in early symptomatic alzheimer disease: The trailblazer-alz 2 randomized clinical trial. *JAMA*, 330(6):512-527.

Sun Y, Xu L, Li Y, et al., 2024. Mitophagy defect mediates the aging-associated hallmarks in hutchinson-gilford progeria syndrome. *Aging Cell*, 23(6):e14143. https://doi.org/10.1111/acel.14143

Tudorica DA, Basak B, Puerta Cordova AS, et al., 2024. A rab7a phosphoswitch coordinates rubicon homology protein regulation of parkin-dependent mitophagy. *J Cell Biol*, 223(7) https://doi.org/10.1083/jcb.202309015

Um J-H, Yun J, 2017. Emerging role of mitophagy in human diseases and physiology. *BMB Reports*, 50(6):299-307. https://doi.org/10.5483/BMBRep.2017.50.6.056

Van Dyck CH, Swanson CJ, Aisen P, et al., 2023. Lecanemab in early alzheimer's disease. *N Engl J Med*, 388(1):9-21. https://doi.org/10.1056/NEJMoa2212948

Walker DG, Lue L-F, 2007. Anti-inflammatory and immune therapy for alzheimer's disease: Current status and future directions. *Curr Neuropharmacol*, 5(4):232-243.

Wang H, Shen M, Ma Y, et al., 2024a. Novel mitophagy inducer alleviates lupus nephritis by reducing myeloid cell activation and autoantigen presentation. *Kidney Int*, 105(4):759-774. https://doi.org/10.1016/j.kint.2023.12.017

Wang M, Yan C, Li X, et al., 2024b. Non-invasive modulation of meningeal lymphatics ameliorates ageing and alzheimer's disease-associated pathology and cognition in mice. *Nat Commun*, 15(1):1453. https://doi.org/10.1038/s41467-024-45656-7

Weissig V, 2020. Drug development for the therapy of mitochondrial diseases. *Trends Mol Med*, 26(1):40-57.
Xu L, 2024. Hippocampal mitophagy contributes to spatial memory via maintaining neurogenesis during the development of mice. *CNS Neurosci Ther*, 30(6):e14800.
Xu X SY, Cen X, Shan B, Zhao Q, Xie T, Wang Z, Hou T, Xue Y, Zhang M, Peng D, Sun Q, Yi C, Najafov a, Xia H. , 2021. Metformin activates chaperone-mediated autophagy and improves disease pathologies in an alzheimer disease mouse model. *Protein Cell*, 12(10):769-787.
Yan M, Li Y, Luo Q, et al., 2022. Mitochondrial damage and activation of the cytosolic DNA sensor cgas-sting pathway lead to cardiac pyroptosis and hypertrophy in diabetic cardiomyopathy mice. *Cell Death Discov*, 8(1):258. https://doi.org/10.1038/s41420-022-01046-w
Yang Y, Jia X, Yang X, et al., 2024. Targeting vdac: A potential therapeutic approach for mitochondrial dysfunction in alzheimer's disease. *Brain Res*, 1835:148920. https://doi.org/10.1016/j.brainres.2024.148920
Yao Z LX, Wang W, Ren P, Song S, Wang H, Xie Y, Li X, Li Z., 2023. Corn peptides attenuate non-alcoholic fatty liver disease via pink1/parkin-mediated mitochondrial autophagy. *Food Nutr Res*, 67
Young ML, Franklin JL, 2019. The mitochondria-targeted antioxidant mitoq inhibits memory loss, neuropathology, and extends lifespan in aged 3xtg-ad mice. *Mol Cell Neurosci*, 101:103409. https://doi.org/10.1016/j.mcn.2019.103409
Zemek F, Drtinova L, Nepovimova E, et al., 2014. Outcomes of alzheimer's disease therapy with acetylcholinesterase inhibitors and memantine. *Expert Opin Drug Saf*, 13(6):759-774. https://doi.org/10.1517/14740338.2014.914168
Zhang J, Kong G, Yang J, et al., 2025a. Pathological mechanisms and treatment progression of alzheimer's disease. *European Journal of Medical Research*, 30(1):625. https://doi.org/10.1186/s40001-025-02886-9
Zhang Q, Zhang W, Yuan X, et al., 2025b. Urolithin a in central nervous system disorders: Therapeutic applications and challenges. *Biomedicines*, 13(7) https://doi.org/10.3390/biomedicines13071553
Zhang R, Yang W, Zhu H, et al., 2023a. Nlrc4 promotes the cgas-sting signaling pathway by facilitating cbl-mediated k63-linked polyubiquitination of tbk1. *J Med Virol*, 95(8):e29013. https://doi.org/10.1002/jmv.29013
Zhang W, 2021. The mitophagy receptor fun14 domain-containing 1 (fundc1): A promising biomarker and potential therapeutic target of human diseases. *Genes Dis*, 8(5):640-654. https://doi.org/10.1016/j.gendis.2020.08.011
Zhang Y, Chen H, Li R, et al., 2023b. Amyloid β-based therapy for alzheimer's disease: Challenges, successes and future. *Signal Transduct Target Ther*, 8(1):248. https://doi.org/10.1038/s41392-023-01484-7
Zhang Z, Li M, Li X, et al., 2024. Glutamine metabolism modulates microglial nlrp3 inflammasome activity through mitophagy in alzheimer's disease. *J Neuroinflammation*, 21(1):261. https://doi.org/10.1186/s12974-024-03254-w
Zhou Q, Cen P, Chen Z, et al., 2025. Roles of the keap1/nrf2 pathway and mitophagy in liver diseases. *J Zhejiang Univ Sci B*, 26(10):972-994. https://doi.org/10.1631/jzus.B2400053
Zhou Y, Liu Y, Kang Z, et al., 2023. Circeps15, as a sponge of mir24-3p ameliorates neuronal damage in parkinson disease through boosting pink1-prkn-mediated mitophagy. *Autophagy*, 19(9):2520-2537. https://doi.org/10.1080/15548627.2023.2196889

Supplementary information

Figs. S1 and S2